Tectonic Evolution of a Sedimented Oceanic Transform Fault: The Owen Transform Fault, Indian Ocean

Alexandre Janin, Nicolas Chamot-Rooke, Matthias Delescluse, Marc Fournier, Jean-Arthur Olive, Alain Rabaute, Philippe Huchon, Jérôme Dyment, Christophe Vigny, Mathieu Rodriguez

Tectonics

RESEARCH ARTICLE
10.1029/2023TC007747

Tectonic Evolution of a Sedimented Oceanic Transform Fault: The Owen Transform Fault, Indian Ocean

Alexandre Janin[1], Nicolas Chamot-Rooke[1], Matthias Delescluse[1], Marc Fournier[2], Jean-Arthur Olive[1], Alain Rabaute[2], Philippe Huchon[2], Jérôme Dyment[3], Christophe Vigny[1], and Mathieu Rodriguez[1]

[1]Laboratoire de Géologie - CNRS UMR 8538, École normale supérieure - PSL University, Paris, France, [2]Sorbonne Université, CNRS-INSU, Institut des Sciences de la Terre de Paris, Paris, France, [3]Université Paris Cité, Institut de physique du globe de Paris, CNRS, Paris, France

Key Points:

- A new set of seismic reflection lines allows time-calibration of the Indus Fan sediments deposited within the Owen transform valley
- The recent tectonic regime includes a still active transpression since 1.5–2.4 Ma that followed a million-years-long period of quiescence
- A nascent median ridge grows south of the fault, a feature found at many other transform faults but captured here in its very early stage

Supporting Information:

Supporting Information may be found in the online version of this article.

Correspondence to:

A. Janin,
alexandre.janin@protonmail.com

Citation:

Janin, A., Chamot-Rooke, N., Delescluse, M., Fournier, M., Olive, J.-A., Rabaute, A., et al. (2023). Tectonic evolution of a sedimented oceanic transform fault: The Owen Transform Fault, Indian Ocean. *Tectonics*, *42*, e2023TC007747. https://doi.org/10.1029/2023TC007747

Received 11 JAN 2023
Accepted 24 APR 2023

Abstract The Owen transform fault (OTF) connecting the Sheba and the Carlsberg spreading ridges in the Indian Ocean currently forms the active plate boundary between India and Somalia plates. This 330-km-long transform fault is by far the longest transform fault along the India-Somalia plate boundary and its valley is buried under the thick distal turbidites of the Indus Fan with total thickness ranging from 1,000 to >5,000 m. A new set of seismic reflection and multibeam bathymetric data reveals remarkable transpressive structures along its entire length recorded as folds in the sedimentary cover, eruption of mud ridges at the seafloor, thrusts in the young oceanic lithosphere. Based on a new regional time-calibration of the seismic reflectors, we show that sediments in the transform valley (post 8.6 Ma) recorded a period of tectonic quiescence until the onset of a transpressive event around 1.5–2.4 Ma that we relate to a minor change in India-Somalia kinematics not captured by magnetic anomalies. This tectonic regime is still active based on compressive earthquakes and deformation of the most recent sediments. Transpression resulted in the formation of a proto-median ridge and the coeval propagation of the tip of the Carlsberg Ridge into the Somalian plate. These features are typically encountered at many other transform faults but rarely captured in their very early stage.

Plain Language Summary Oceanic transform faults are tectonic plate boundaries along which two plates slide against each other. Often located far from sediment sources, oceanic transform faults are essentially sediment-free and their geological evolution can only be addressed using past Earth magnetic field inversions recorded in the seafloor basaltic rocks, leading to a time resolution no better than several million years. We report here new findings obtained at the active Owen Transform Fault, the longest oceanic transform faults between India and Somalia plates. Indus Fan sediments derived from the western Himalaya erosion have accumulated with time in a deep valley adjacent to the Owen Transform Fault, offering a unique high-resolution stratigraphic record of past regional tectonics. The analysis of seismic reflection profiles across this valley reveals that the Owen Transform Fault is under a transpressive regime since 1.5–2.4 Ma, unpredicted by magnetics-based India-Somalia kinematics. This unusual regime for a supposedly pure strike-slip fault is still active as shown by thrust earthquakes and deformation of the most recent sediments. We discuss the origin of similar structures found at long-lived oceanic transform faults in other oceans, and propose that subtle changes in plate motion may be responsible.

1. Introduction

Plate tectonics theory predicts that transform faults connecting mid-oceanic ridge segments are long-lasting steady-state features, since their length, side-to-side material contrast, rate and style are invariant as long as boundary conditions remain stable. In nature, transform faults formed in the early stage of oceanic basin opening commonly have lifespans of several tens of million years (Bonatti et al., 1994; Géli et al., 1997; Maia et al., 2016), in agreement with the theory. Furthermore, global plate models for past and current kinematics based on magnetics and geodesy point to relative kinematic stability over the last million years (DeMets et al., 2010), within the bounds of data uncertainties (such as errors in fault traces, magnetic pickings, focal mechanisms, GPS measurements).

Yet, the multi-strand morphology of some of the longest transform faults bears witness to a complex geological evolution involving fault abandonment, fault growth, uplift of transverse and median ridges, formation of

intra-transform spreading centers. These structures have generally been interpreted as transient and resulting from either global plate kinematic reorganizations or local plate boundary evolution (Bonatti, 1978; Harmon et al., 2018; Lodolo et al., 2013; Maia, 2019; McCarthy et al., 1996; Menard & Atwater, 1969; Pockalny et al., 1996, 1997). Although some of these unusual features seem to correlate with regional tectonic events, the details of the tectonic accommodation of new plate-scale boundary conditions remain elusive. The use of magnetics to follow transform faults tectonics is itself limited since chron identification provides snapshots with a time step of the order of a million years. Beyond plates-related events, the steady-state regime of oceanic transform faults is still prone to discussion, with issues such as the tectonic regime (Grevemeyer et al., 2021; Mishra & Gordon, 2016; Ren et al., 2022), the width of the accommodation zone (Ligi et al., 2002), the role of fluid circulation (Kohli & Warren, 2020; Kohli et al., 2021; Prigent et al., 2020), the thermal regime (Behn et al., 2007; Sandwell, 1986; Turcotte, 1974; Wessel & Haxby, 1990), the Ridge-Transform Intersection (RTI) tectonics (Cann et al., 1997; Fox & Gallo, 1984; Morgan & Parmentier, 1984; Severinghaus & Macdonald, 1988), the variability of the nature of the crust (Guo et al., 2023; Marjanović et al., 2020), the role of the absolute motion with respect to the mantle (Cormier & Sloan, 2019). Little is known about the short-term evolution of oceanic transform faults at the million-year timescale, simply because time and tectonic markers are missing.

Often located far from the sediment sources, oceanic transform faults are essentially sediment-free, or at best covered by a thin pelagic blanket draping the crustal rocks (such as the Chain Fracture Zone, Agius et al., 2018; Harmon et al., 2018). At many transform faults, the entire record of the tectonic history is condensed within a sedimentary column not exceeding a few hundred meters, generally not time-calibrated due to the sparsity of deep-sea drillings. In this study, we take advantage of the particular tectono-sedimentary setting of one major oceanic transform fault, the Owen Transform Fault in the northwestern Indian Ocean. Located at the western termination of the Carlsberg Ridge, this 330-km-long fault is part of the active plate boundary between India and Somalia. A key property of the Owen Transform Fault is that the transform fault valley is the far-end depocentre for the distal Indus turbidites (Figure 1), bearing resemblance to the Vema Transform Fault valley fed by the Amazon Cone and filled with ∼1,000 m of sediments (Bonatti et al., 2003, 2005; Perch-Nielsen et al., 1977). The Owen Transform Fault however represents an end-member case of a sedimented transform fault, with more than 5,000 m of sediments piled in the valley at its deepest point, providing an exceptional sedimentary record of the tectonic events through time.

The new set of marine data used here was collected in 2019 during the VARUNA and CARLMAG cruises aboard *BHO Beautemps-Beaupré*, an oceanographic ship operated by the French Naval Hydrographic and Oceanographic Services (SHOM) and the French Navy. The entire length of the active Owen Transform Fault was surveyed resulting in a near 100%-coverage multibeam bathymetry. A set of high-resolution seismic lines was acquired both across and along the fault, revealing the past and present-day deformation recorded in the sediments. The fault presently runs along a narrow corridor and was recently subjected to pulses of transpression recorded as unconformities. Using the seismic lines calibrated at ODP and DSDP drilling sites, the main phases of deformation are dated and their possible origin is discussed.

2. Geological Background

2.1. Spreading History at the Carlsberg Ridge and the Origin of the Owen Transform Fault

The Carlsberg Ridge and the Owen Transform Fault constitute the current India-Somalia plate boundary (Figure 1a). The Cenozoic history of opening in this part of the Indian Ocean is well recorded by magnetic anomalies identified in the Arabian Sea and on both sides of the Carlsberg and Sheba Ridges (Figure 1b). Seafloor spreading at the Carlsberg Ridge started at Chron 28 (∼63 Ma) in the wake of the India-Seychelles breakup (Chaubey et al., 1998; Dyment, 1998). The spreading regime was ultra-fast, with a rate of ∼15 cm yr^{-1} until Chron 22 (∼50 Ma) from which the spreading rate decreased drastically by ∼90% around Chron 20 (∼44 Ma, Mercuriev et al., 1995; Dyment, 1998; Chaubey et al., 2002) or Chron 21 (∼47.2 Ma, DeMets and Merkouriev, 2021) following the India-Eurasia collision. After Chron 20, the Carlsberg Ridge entered a period of slow spreading and possibly ultra-slow at its intersection with the Owen Transform Fault, the Carlsberg-Owen RTI being the closest point to the India-Somalia pole of opening along the Carlsberg ridge. During this period, the spreading direction rotated clockwise (DeMets & Merkouriev, 2021; Mercuriev et al., 1995) and the spreading rate was close to 1 cm yr^{-1} (DeMets & Merkouriev, 2021). The ultra-slow spreading period ended around 22 Ma and after a short period of moderate fluctuation, the spreading rate stabilized to the present-day value of ∼21 mm yr^{-1} at

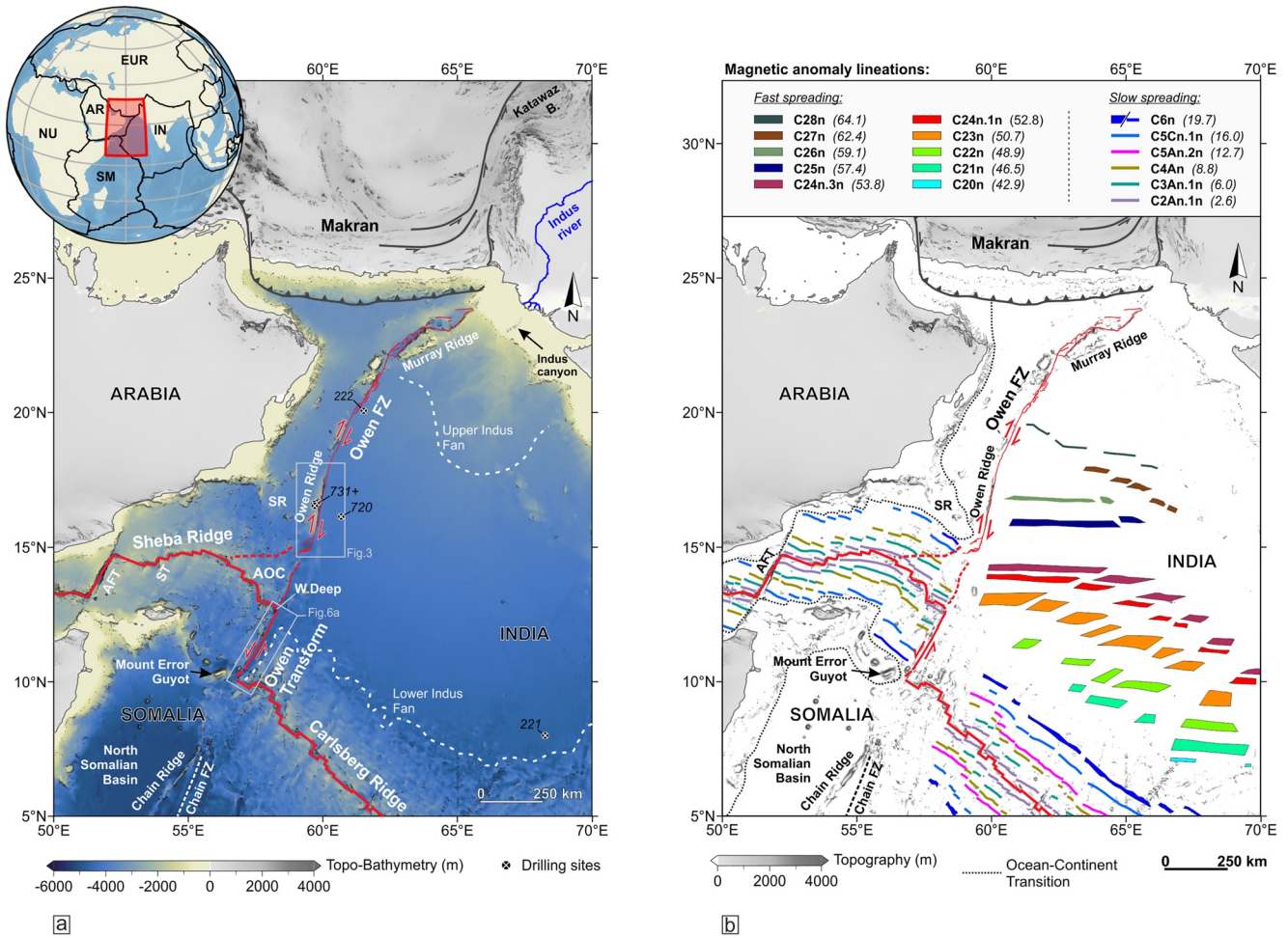

Figure 1. Simplified geodynamic setting of the Arabian Sea. Topography/bathymetry grid is SRTM30_PLUS (Becker et al., 2009). Identifiers next to the drilling sites refer to site numbers: 221 and 222 for DSDP Leg 23; 720 for ODP Leg 117; the site quoted 731+ corresponds to a series of sites on the top of the Owen Ridge detailed in Figure 3. In insert, the global plate boundaries model of Bird (2003): AR, Arabia; EUR, Eurasia; IN, India; NU, Nubia; SM, Somalia. (b) Simplified seafloor magnetic anomaly lineations map (in the Arabia Sea, C28n-C20n from Chaubey et al. (2002), C6n-C2An.1n from Merkouriev and DeMets (2006); in the Gulf of Aden from Fournier et al. (2010)). Between parenthesis, the age of the picked chrons in Ma. AFT, Alula-Fartak Transform fault; AOC, Aden-Owen-Carlsberg triple junction; B, Basin; FZ, Fracture Zone; SR, Sharbitat Ridge; ST, Socotra Transform fault; W.Deep, Wheatley Deep.

the Carlsberg-Owen RTI (DeMets et al., 2020; DeMets & Merkouriev, 2021; Mercuriev et al., 1995; Merkouriev & DeMets, 2006).

Accretion at the Carlsberg Ridge has been accompanied by the transcurrent motion of India relative to adjacent plates (Africa and Arabia), recorded in the present-day seafloor of the Arabian Sea as prominent linear ridges such as the Chain Ridge and the Owen Ridge (Figure 1, Fournier et al., 2011; Rodriguez, Chamot-Rooke, Huchon, Fournier, & Delescluse, 2014; Rodriguez et al., 2011, 2016). During the Paleocene-Eocene period, strike-slip motion between India and Africa was along the Chain Fracture Zone (Figure 1, Royer et al., 2002; Rodriguez et al., 2016). The transcurrent plate boundary then evolved with the fragmentation of Africa into three distinct plates (Arabia, Somalia, Nubia) and the concomitant opening of the Red Sea and Gulf of Aden along the Sheba Ridge (Bellahsen et al., 2003; Bosworth et al., 2005; Leroy et al., 2012; McQuarrie et al., 2003). The formation of the modern Owen Transform Fault connecting the Sheba and the Carlsberg Ridges is coeval with this major Oligo-Miocene reconfiguration, Sheba's tip propagating rapidly into the Afro-Arabian continent toward the Afar plume (Bellahsen et al., 2003; Cochran, 1981; Hubert-Ferrari et al., 2003; Manighetti et al., 1997; Steckler and ten Brink, 1986).

Changes in the Carlsberg Ridge spreading rate correlate with some of the main events that punctuated the opening of the Indian Ocean: fast spreading during the migration of India toward Eurasia, decreasing rates following

the collision (Patriat & Achache, 1984), ultra-slow spreading (Mercuriev et al., 1995) following the reorganisation of the Indian Ocean spreading ridge system with the abandonment of the Wharton Ridge (Jacob et al., 2014), and close to present-day rates since the opening of the Gulf of Aden (DeMets et al., 2020). According to the latest plate reconstructions based on magnetic data (DeMets & Merkouriev, 2021), India-Somalia motion remained in a quasi steady-state regime since 13 Ma, at least in rate. On the other hand, the predicted direction of opening based on the same reconstructions shows strong scattering. Accretion at the Carlsberg Ridge seems to have been insensitive to tectonic events nearby, such as the initiation of slow intraplate deformation in the Central Indian Ocean around 15 Ma and its acceleration around 8–9 Ma (Bull et al., 2010; Delescluse et al., 2008; Stevens et al., 2020) or the late Miocene uplift of the Owen Ridge and Murray Ridge (Gaedicke et al., 2002; Rodriguez, Chamot-Rooke, Huchon, Fournier, & Delescluse, 2014). At the level of precision of the magnetic data, steady boundary conditions seem to have prevailed at the Owen Transform Fault since 12.5 Ma (DeMets & Merkouriev, 2021).

2.2. Turbiditic System of the Indus Fan: Implications for the Distal Sedimentation

Sediments trapped in the Owen Transform Fault valley are recent, but no age has been proposed so far. The age of the modern Indus Fan initiation itself is still subject to discussion due to the scarcity of deep drilling in the Arabian Sea (Clift et al., 2001, 2002; Najman, 2006). According to Qayyum et al. (1996, 1997), early Eocene products of the erosion of the nascent western Himalayan mountains were feeding longitudinally a proto-fan west of the northern Indian margin, carried by a paleo-Indus river. The corresponding turbiditic and deltaic sediments, known as the Khojak Fan formation, are now exposed in the Katawaz basin, Pakistan (Qayyum et al., 1996, Figure 1). An early Oligocene age was assigned to the base of this formation (Carter et al., 2010), slightly younger than the late Eocene age proposed in earlier studies, compatible with the Paleogene to Neogene shift in the fan position proposed in Qayyum et al. (2001). The early drainage pattern may have been diverted to the east by the uplift of the Murray Ridge (Edwards et al., 2000), which seems to have been a multiphase process. Several growth pulses have been recognized starting in the Paleocene (Clift et al., 2001; Gaedicke et al., 2002) and peaking in the middle to late Miocene (Mountain & Prell, 1990; Rodriguez, Chamot-Rooke, Huchon, Fournier, Lallemant, et al., 2014). A sharp increase in the terrigenous influx toward the Arabian Abyssal Plain occurred in the early Miocene (Davies et al., 1995) or middle Miocene (Rea, 1992), but clays sedimentation in the northern Arabian Sea issued from the Indus River may have started earlier in the late Oligocene (Kolla & Coumes, 1987; Weedon and McCave, 1991).

Based on multichannel seismic lines around the Murray Ridge tentatively tied to industrial wells, an Eocene age was proposed for the deepest turbiditic series of the modern fan in the Arabian Sea (Clift, 2006; Clift et al., 2002). A Paleogene age for the distal Indus Fan was inferred based on pre-Miocene turbidites found as far south as the southern tip of the Owen Ridge at ODP sites (all sites are located in Figures 1 and 2). However, the origin of these turbidites remains controversial, and a western Arabian source - rather than eastern Indian - has also been proposed for the Oligocene-Eocene turbidites drilled at site 224 (Jipa and Kidd, 1974; Mallik, 1974; Najman, 2006; Whitmarsh et al., 1974a). One single ODP drill recovered the entire sediment pile covering the northern flank of the Carlsberg Ridge, reaching a tholeiitic basement Middle Eocene in age (site 221, Whitmarsh et al., 1974b, location in Figure 1). Earliest Indus-derived sediments were found to be late Oligocene above pelagic Paleogene oozes (Weser, 1974). The proportion of pre-Miocene fan turbidites in the Arabian Sea remains largely unknown, but it is expected that most, if not all, distal sediments are post-Paleogene.

The present-day morphology of the proximal (upper) Indus Fan is marked by large channel-levee systems (Kolla & Coumes, 1987; Mishra et al., 2016; Von Rad & Tahir, 1997), while over the distal (lower) Indus Fan system, levees become smaller, channels are less numerous and the distance between channels increases (Kolla & Coumes, 1987). Far from the sources, the sedimentary cover is thus marked by an alternation of turbidites (in the vicinity of an active turbiditic channel) and pelagites (when channels migration took them further) (Shipboard Scientific Party, 1989a; Von Rad & Tahir, 1997). In the very distal domain, poorly channelized turbidites gently onlap the northern flank of the Carlsberg Ridge far from the ridge axis; a fraction of them find their way further south along the Owen Transform and are finally trapped in the valley.

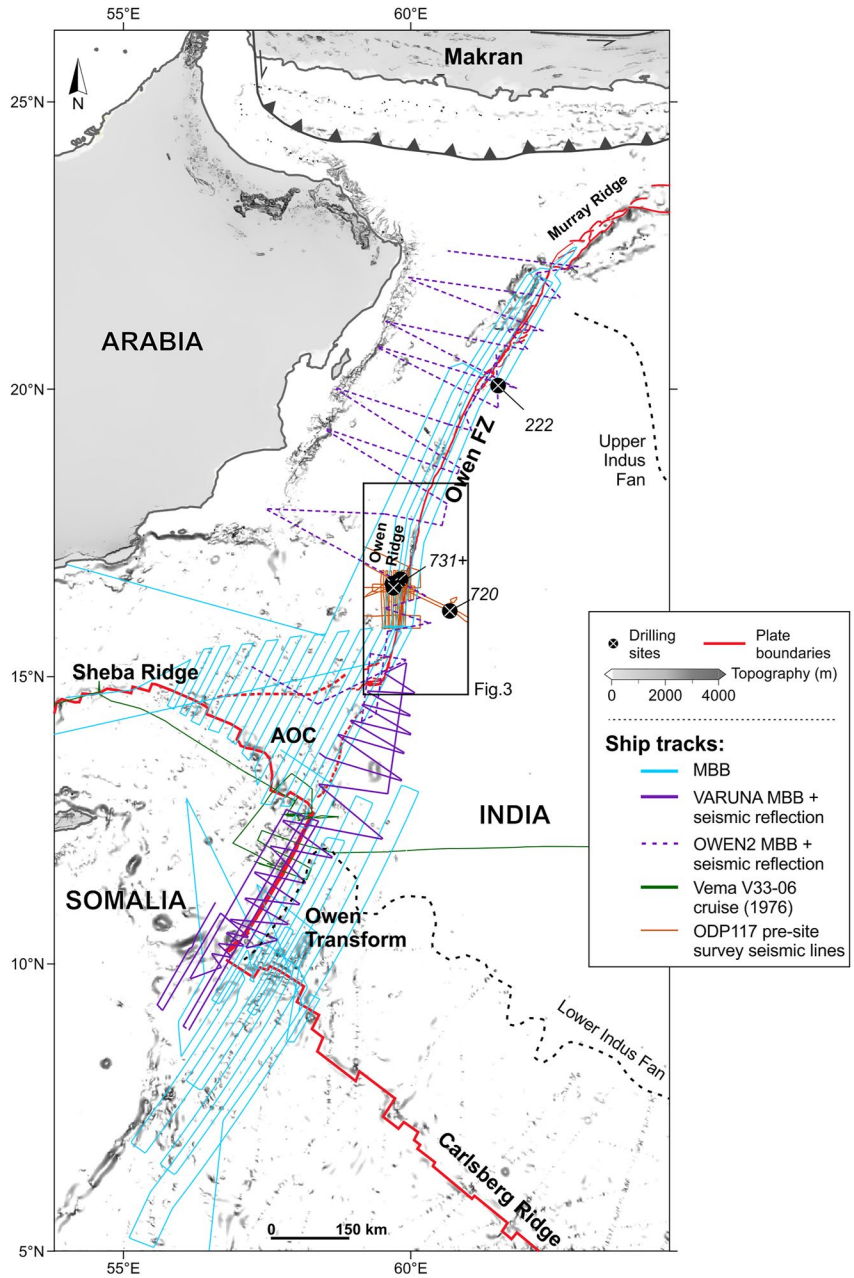

Figure 2. Cruise tracks used in this study. In blue, multi-beam bathymetry (MBB) and in purple, both MBB and seismic reflection. AOC, Aden-Owen-Carlsberg triple junction; FZ, Fracture Zone.

3. Data

3.1. Previous Surveys Across the Owen Transform Fault

Two vintage seismic profiles were shot in the late 1970s during the Lamont-Doherty Earth Observatory cruise V33-06 (1976, see track location in Figure 2) across the northern segment of the Owen Transform Fault aiming at identifying steep scarps for dredging (Bonatti et al., 1983; Bonatti & Hamlyn, 1978). Ultramafics rocks outcrop along the entire length of the western wall of the Wheatley Deep (Hamlyn & Bonatti, 1980), up to the very top of a 4 km high scarp which proved later to be an inside corner oceanic core complex formed at the Sheba Ridge (Fournier et al., 2010). Sepiolite deposits were recovered further south along another steep scarp (Bonatti et al., 1983), interpreted as the result of seawater circulating at crustal depth and interacting with ultramafic rocks

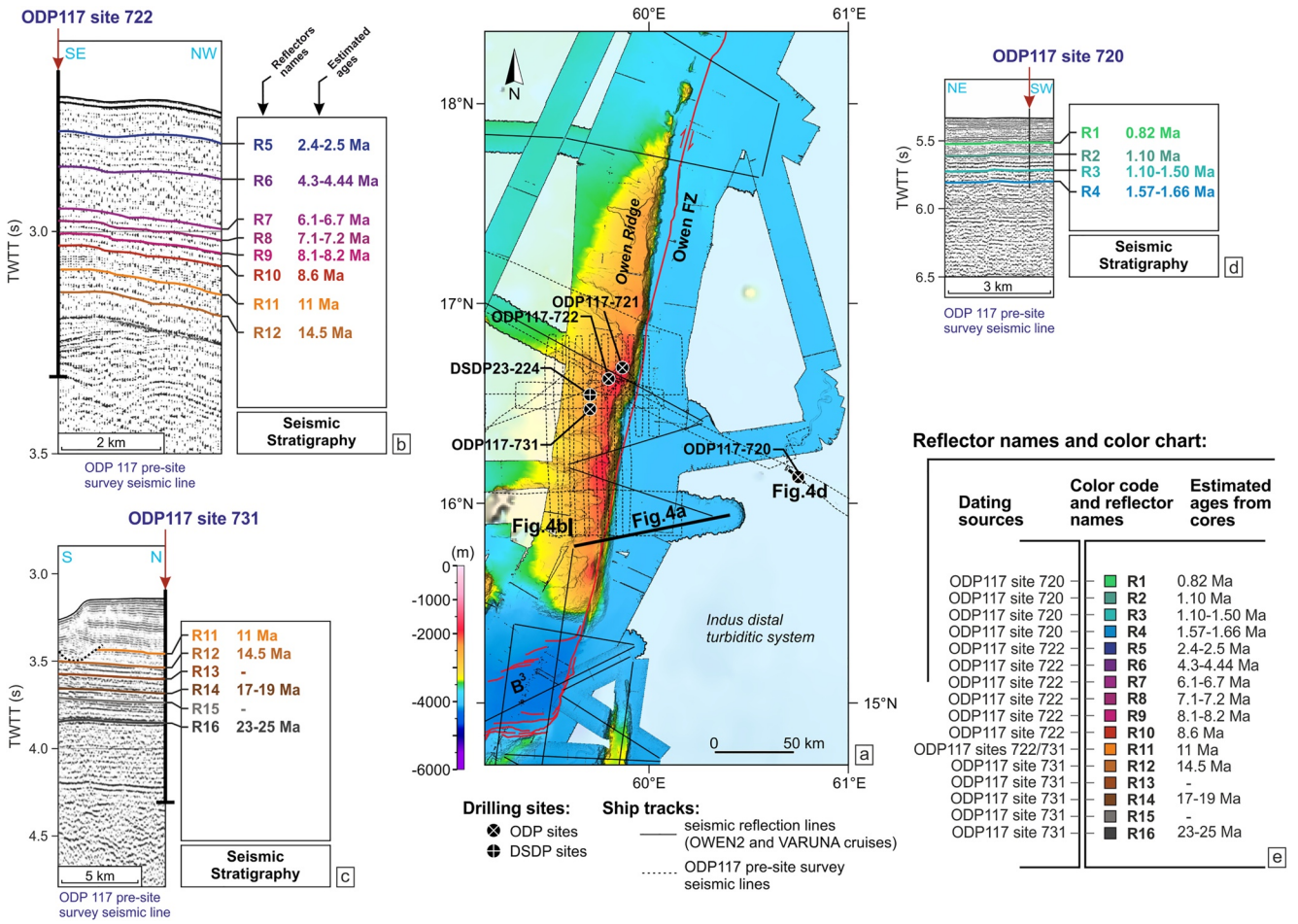

Figure 3. Seismic stratigraphy and time-calibration of reflectors on ODP seismic profiles. (a) Location map of drilling sites and seismic lines. In red, the Owen Fracture Zone active trace from Rodriguez et al. (2011, 2018). Multibeam is complemented with SRTM30_PLUS in the background (Becker et al., 2009). The thick black lines show the location of the seismic lines displayed in Figure 4. (b–d) Time-calibration summaries at sites 731, 720, and 722 of ODP Leg 117, respectively. (e) Table summarizing the dated reflector names and the associated color chart used in this study. B^3, Beautemps-Beaupré Basin; FZ, Fracture Zone.

before shallow precipitation along fault planes. No further marine survey has been specifically devoted to the Owen Transform Fault since the advent of modern oceanographic ships.

3.2. The New Data Set

The Bathymetric grid used in this study is a compilation of bathymetric data from previous cruises on this region (Figure 2): AOC (https://doi.org/10.17600/6090030), OWEN (https://doi.org/10.17600/9090020), OWEN-2 (https://doi.org/10.17600/12090050) plus the new VARUNA (https://doi.org/10.17600/18001108) and CARL-MAG (https://doi.org/10.17600/18000872) data. All data were acquired with the same Kongsberg-Simrad EM120 deep-water multibeam echo-sounder aboard *BHO Beautemps-Beaupré* oceanographic ship. Grids were built at 10- to 50-m horizontal spacing, with a vertical resolution of about 10 m.

VARUNA seismic reflection profiles (Figure 2) were acquired at 10 knots ship speed (fast acquisition) using two coupled air-guns of 45/45 c.i. and 105/105 c.i. fired every 10 s allowing a 9 s record length. Acquisition on a 300-m long 48-channel streamer allows a theoretical Common Mid-Point spacing of 3.125 m. The entire seismic data set (5,000 km in total) was processed using the CGG Geovation software. Processing consisted of Normal Move-Out correction, stacking, bandpass filters (13-16-100-125 Hz) and migration (Kirchoff migration, mostly using water velocity, with local variations to improve imaging where needed). The imaged profiles show good penetration down to the basement, sometimes reaching the very limit of the record at 9 s two-way travel time. Some of the profiles acquired previously during the OWEN-2 cruise (Figure 2) were reprocessed to improve ties between the two surveys.

Sub-Bottom seismic Profiler (SBP hereafter) was used to characterize the geometry of recent sediment deposits (the first ~0.2 s two-way travel time) and discuss faults activity. Profiler data were corrected for recording delay and amplitudes were tuned via Automatic Gain Control and signal normalization.

4. Calibration of the Distal Indus Turbiditic Sediments

The drilling sites closest to the Owen Transform Fault are located near the Owen Ridge, some 400 km away from the northern entry of the fault valley (Figure 2). The paleo-faunal and magnetostratigraphy studies at ODP (Shipboard Scientific Party, 1989d) and DSDP (Whitmarsh et al., 1974a) sites provided a chronostratigraphic framework, which formed the basis of all subsequent studies dealing with the middle and distal Indus Fan. In the following sections, we (a) update the time-calibration of seismic profiles acquired as pre-site surveys at ODP sites, (b) gather available calibrations onto a regional seismic reference line running from the Owen Ridge to the distal/middle Indus turbiditic system, and finally (c) propagate the reflectors calibration south in the Owen Transform Fault valley using the new set of VARUNA seismic lines.

4.1. Calibration at ODP Sites

Hole 720 (ODP leg 117) is the only regional drill site located over the current middle/distal Indus turbiditic system (Figure 3a). The sedimentary cover is typically composed of turbidites/pelagites alternations, at least in the upper portion since drilling stopped in the upper Pleistocene (Shipboard Scientific Party, 1989a). Four additional drill sites are located on the top of the Owen Ridge (Figure 3a): sites 721, 722, and 731 of ODP expedition 117 (Shipboard Scientific Party, 1989c, 1989d) plus site 224 of DSDP expedition 23. Turbidite sequences have been recovered from their base, switching progressively to pelagites upward with the uplift of the Owen Ridge above the level of turbidite deposition in the late Miocene (Rodriguez, Chamot-Rooke, Huchon, Fournier, & Delescluse, 2014; Shipboard Scientific Party, 1989b, 1989c, 1989d).

Calibrations at sites 722, 731, and 720 (ODP leg 117) are shown in Figures 3b–3d, respectively (details for age assignment, seismic reflectors identification and time-depth conversion are given Figures S1–S3 and Text S1–S3 in Supporting Information S1). Four high-amplitude seismic reflectors identified regionally were calibrated at site 720 (labeled from R1 for the youngest one to R4 for the oldest one), ranging in age from 0.82 Ma to 1.57–1.66 Ma (Figure 3d). Ten additional reflectors have been recognized and calibrated on the top of the Owen ridge at sites 722 and 731 (labeled R5 to R16, Figures 3b and 3c), spanning the entire lifetime of the Owen Transform Fault from 2.4 to 2.5 Ma to 23–25 Ma.

4.2. Link Between the Indus Turbiditic System and the Owen Ridge Units

Calibrating the deepest horizons in the abyssal plain requires a tie between the well-calibrated units at the top of the Owen Ridge and the thick sediment pile in the plain itself. One East-West seismic line acquired during the OWEN-2 cruise runs from the Owen Ridge to the Indus Fan (Figure 4, location in Figure 3a), crossing the Owen Fracture Zone scarp in the vicinity of the ODP drilling sites near 15.9°N. We use it as a reference line for calibration.

Recent abyssal plain reflectors are tied to site 720 (R1-R4, Figure 4d) while reflectors located at the top of the Owen Ridge are tied to site 731 along the flank of the Owen Ridge (Figure 4b, the full reflector tracking is given in the Figure S4 in Supporting Information S1). The pre-uplift Miocene sedimentary units on the top of the ridge (bracketed between 23 and 25 Ma (R16) and 11 Ma (R11)) cannot be simply followed down to the abyssal plain since correlation requires jumping from one side of the Owen Fracture Zone scarp to the other side (Figures 4a and 4b). However, a set of tilted reflectors imaged at the foot of the scarp (Figure 4a, zoom panel 2) shows seismic facies similarities with those recognized at the top of the ridge. The deepest part of this tilted section is composed of a thick (~1 sTWTT) transparent unit covered by a series of high-amplitude reflectors, which correlates with the pre-uplift Miocene sedimentary cover identified on the top of the ridge. Figure 4c shows that the correlation is robust. Once recognized within the tilted unit, the Miocene R11-R16 sequence can be followed along the remaining distal portion of the reference line. Figure 4e shows the detailed interpretation of the reference line and the position of the entire set of reflectors.

East of the tilted sedimentary unit, gently folded and faulted sediments form a positive flower structure (Figures 4a and 4e, zoom panel 4) previously interpreted as the former trace of the Arabia-India plate boundary

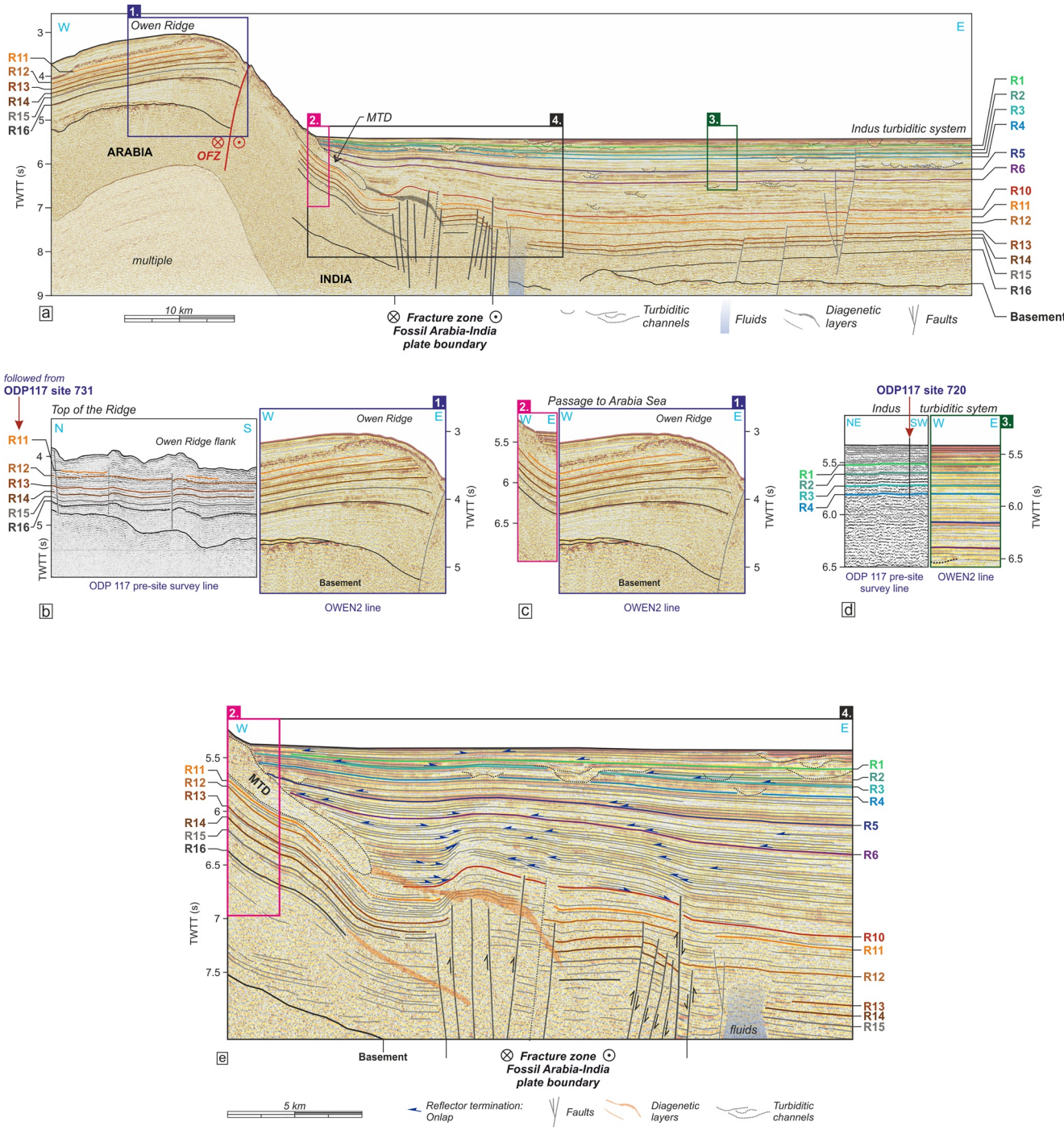

Figure 4. Calibration of the OWEN reference seismic line crossing the Owen Ridge and the Arabian abyssal plain. Location in Figure 3a. (a) Interpreted seismic line. Numbers 1 to 4 refer to the colored zoom panels. (b) Correlation between the ODP pre-site survey line and the OWEN reference line (see Figure S4 in Supporting Information S1). (c) Correlation between reflectors on the top of the Owen Ridge and within the tilted unit. (d) Correlation in the Indus turbditic system between the ODP Leg 117 pre-site survey line crossing the site 720 and the OWEN reference line. (e) Interpreted zoom on reflectors at the bottom of the Owen Ridge (panel 4). MTD, Mass Transport Deposit. Reflectors names refer to Figure 3e. Raw profiles are available in Figures S5 and S6 in Supporting Information S1.

before relocation to its current position ~2.4 Myr ago (Rodriguez, Chamot-Rooke, Huchon, Fournier, & Delescluse, 2014). Onlaps recorded the growth of this structure since the deposition of R10 (red reflector in Figure 4e). Furthermore, a mass transport deposit covers the previously described tilted unit. This MTD is no younger than the red R10 reflector (Figure 4e) since all subsequent series unconformably onlap the chaotic

deposit. A reasonable interpretation is that it was triggered by the uplift of the then nascent Owen Ridge and slid from its flank. Reflector R10 would thus mark the onset of the Owen Ridge uplift around 8.6 Ma (Rodriguez, Chamot-Rooke, Huchon, Fournier, & Delescluse, 2014).

We further identify two distinct unconformities between R4 and R10 within the abyssal plain sequence, capturing several onlap terminations (purple and dark blue reflectors in Figures 4a and 4e). These two reflectors are followed from line to line up to the far site 222 of DSDP leg 23 (Whitmarsh et al., 1974c, location on Figure 2, details in the Figure S3 in Supporting Information S1). This additional long-distance correlation allows us to estimate the age of the dark blue reflector around 2.4 Ma and that of the purple reflector between 3.6 and 5 Ma. Therefore, the dark blue is R5 recognized at site 722 (Figure 3b). We further propose that the purple reflector is R6 (Figure 3b).

4.3. Calibration of the Owen Transform Fault Valley Sediments

The proposed calibration opens a time window over the last 25 Myr of the distal Indus Fan sedimentation, covering the entire life of the Owen Transform Fault but essentially north of it. The final step of the correlation work consists in propagating the calibration south toward the Owen Transform Fault valley. Figure 5a shows the seismic profiles used to tie the full-set of VARUNA seismic lines, from the reference line down to the flank of the Carlsberg Ridge. Calibrated reflectors identified on the reference line (Figure 4) are tracked line by line through the VARUNA network. Figure 5b puts side by side six extracts of the seismic lines with the same vertical scale, aligned with the seafloor and displayed as snapshots along the calibration path. Several units constitute strong constraints for our correlations: R3 marks the base of a high amplitude unit, R5-R6 delimit a finely stratified unit characterized by low amplitude reflectors, and R10 represents the base of a unit with a transparent facies.

Seafloor gently deepens southward as expected for the distal Indus Fan while the total sediment pile gets thinner as the basement gets correlatively younger. At 16°N (Figure 5b, panel A), the deepest calibrated reflector is R16 (23 –25 Ma) above a 57–58 Ma old Paleocene basement (based on magnetics, Figure 1b), the rest of the section below remains undated. At 13°N (Figure 5b, panel D), the Eocene basement (42–43 Ma, DeMets and Merkouriev, 2021) is immediately topped by R14 or R15 (17–19 Ma), suggesting non-deposition during the Paleogene or an abnormally high basement escaping sedimentation before the Miocene flooding. More generally, seismic lines show significant variations of the basement morphology, so that age of the earliest deposits varies from place to place (Figure 5b). At the northern entry of the transform fault valley (Figure 5b, panel F), the deepest calibrated reflector is R6 (4.3–4.44 Ma) whereas laterally (Figure 5b, panel E), the sediments cover is twice thicker and the oldest calibrated reflector is R10 (8.6 Ma).

5. Results

5.1. Morphology of the Owen Transform Fault

The trace of the Owen Transform Fault is sharp in the bathymetry (Figure 6a) and bounds the same structural elements along its entire length: a narrow (5–10-km-wide) deep terrace to the west (labeled Somalian terrace, Figures 6b and 6c), a wide flexural transform fault basin to the east, and an in-between ridge standing above the flat seafloor around (Figure 6a). The transform fault valley is a 30-km-wide 300-km-long depression floored by the Indian oceanic lithosphere and extending from ∼12.3°N to nearly the Carlsberg Ridge axis (Figure 6a). This basin is fed from the north by the distal turbidites of the Indus Fan (Figure 1) while at the same time, new oceanic floor is being formed at the Carlsberg Ridge to the south. To the east, sediments are invading the complicated reliefs formed at the Carlsberg Ridge. To the west, the transform fault valley is abruptly interrupted by a continuous ridge delimiting a bathymetric step between India and Somalia and isolating a deep terrace or suspended basin at the foot of the elevated oceanic crust formed at the Sheba Ridge. Notice that the topographic step between the Somalian plate to the west and the Indian plate to the east does not revert halfway along the transform, as it would for a conventional transform fault: the Sheba side is consistently and significantly shallower than the Carlsberg side. This observation will be further addressed in the discussion section.

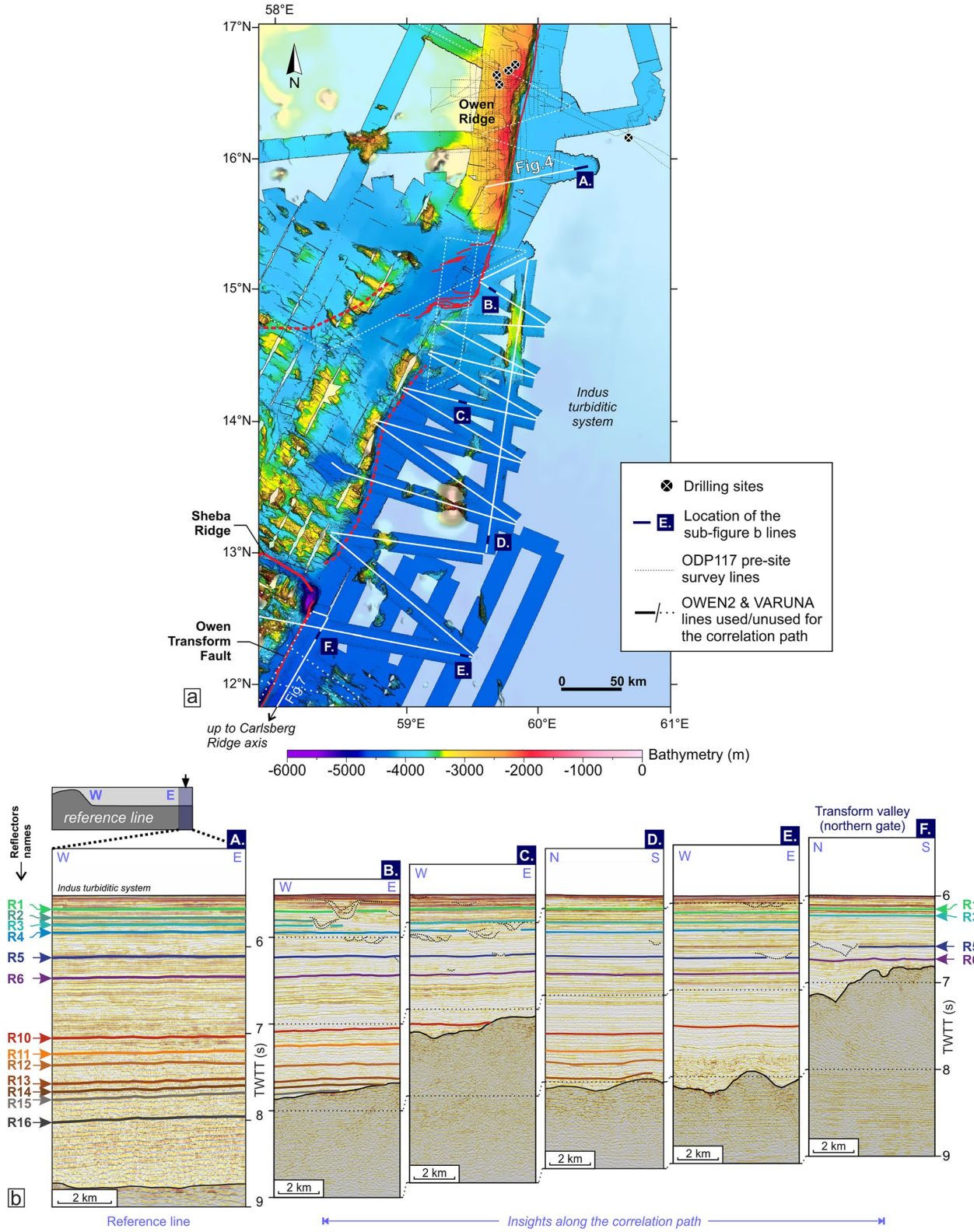

Figure 5. Southward propagation of the calibration from the OWEN reference line to the Owen Transform Fault valley. (a) Bathymetric map showing the seismic lines used as calibration path to reach the sediments deposited into the Owen Transform Fault valley from the OWEN reference line (Figure 4). (b) Six seismic profile segments displayed with the same vertical scale and labeled A-F, distributed along the calibration path.

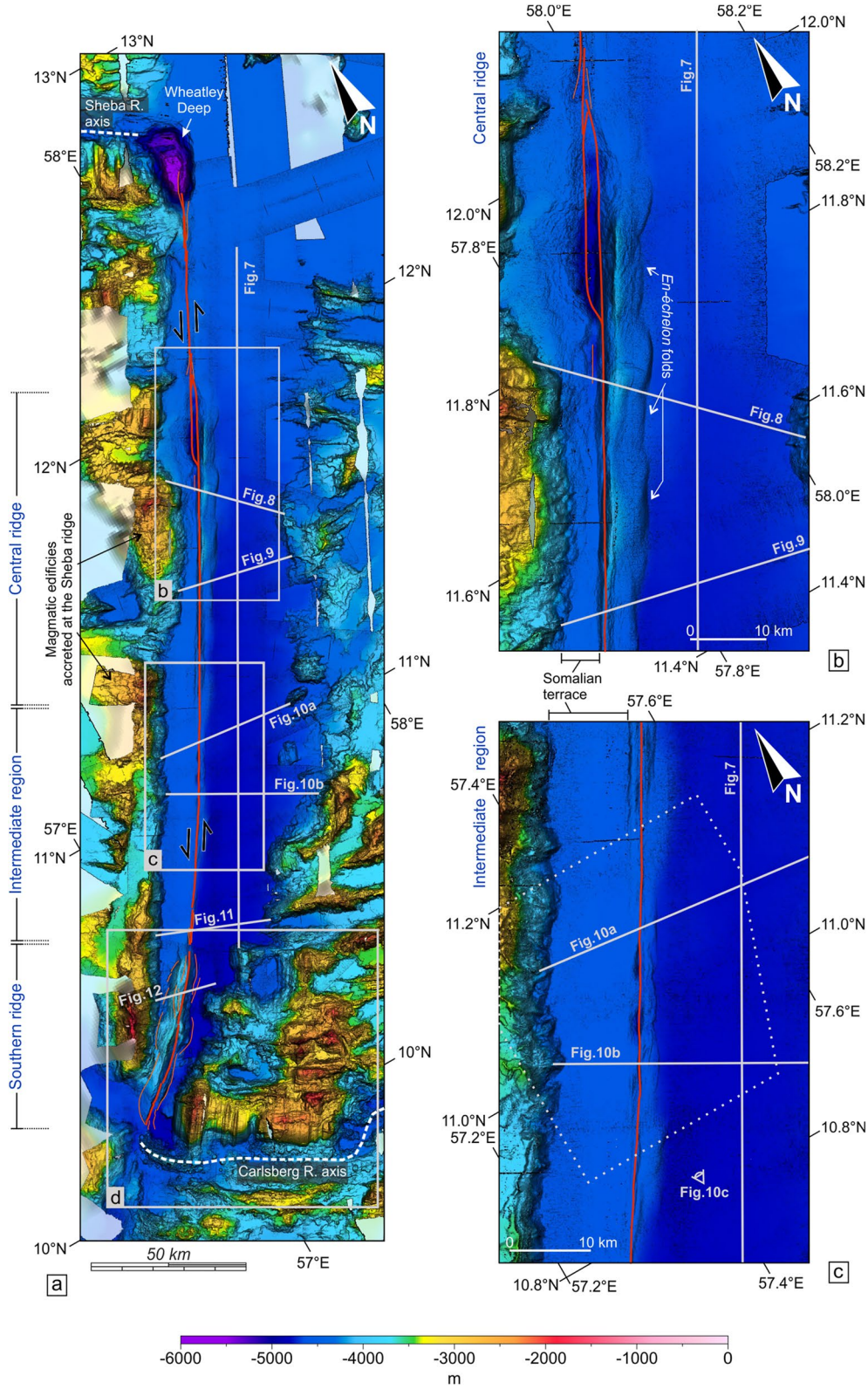

Figure 6. Morphology of the Owen Transform Fault. Map projection: rotated Standard Mercator. (a) Bathymetry of the entire Owen Transform Fault. (b) Zoom on the central ridge. (c) Zoom on the intermediate region. (d) Zoom on the southern ridge. Solid light gray lines are VARUNA seismic tracks. Red lines are active faults. The tight white dashed lines delimit corrugated surfaces. The spaced white dashed lines show the cartographic extent of Figures 10c and 13, their orientations are indicated by "eyes" on the map.

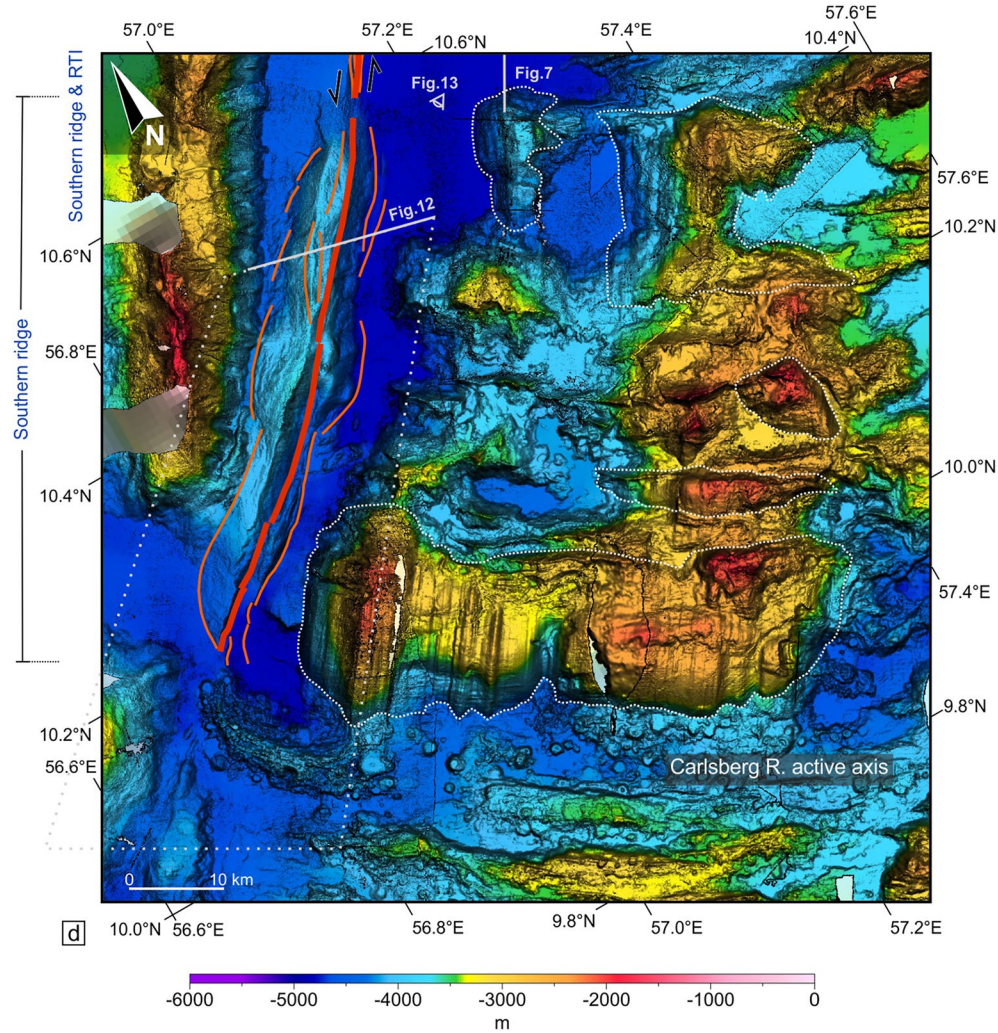

Figure 6. (Continued)

The anticlinal ridge that follows the active trace of the Owen Transform Fault can be subdivided into three segments based on its morphology (Figure 6a):

1. The central ridge (~100 km from 12.0°N to at least 11.2°N) lies on the Indian plate (Figure 6b). The ridge culminates 540 m above the Indian seafloor in its northern part. In detail, the ridge is formed by a series of overlapping en-échelon folds, with fold axes at an acute angle to the trace of the strike-slip fault (Figure 6b).
2. The southern ridge (~65 km from 10.2°N to 10.6°N) is located in the vicinity of the Carlsberg Ridge-Transform-Intersection (Figure 6d). It lies ~1,000 m above the Indian seafloor. The bathymetry shows a system of subsidiary faults cutting the sedimentary cover. In contrast with the sharp trace of the Owen Transform Fault over the central ridge, the surface morphology shows several fault strands (Figure 6d).
3. In the intermediate region located between the central and the southern ridge (~10.6°N and ~11.2°N) the axial ridge is only several tens of meters above the Somalian seafloor (Figure 6c). However, the bathymetric step is preserved across the transform fault and the Somalian seafloor is higher than the Indian seafloor.

The two Ridge-Transform Intersections (RTIs) of the Owen Transform Fault are morphologically very distinct:

1. To the north, the Wheatley Deep is a 1,400 m-deep depression, 15 km-wide and 30 km-long nodal basin that forms the current Sheba-Owen RTI (Fournier et al., 2010, Figure 6a). The deepest point of this basin is around 5,845 m depth. The basin recently escaped turbiditic sedimentation due to a slight basement uplift that deflected the sedimentary flux east of it.

2. To the south, a large 54 km-wide 18–24 km-long corrugated surface occupies most of the oceanic floor on the Indian side at the Carlsberg-Owen RTI (Figure 6d), interpreted as the youngest OCC. Numerous small volcanic cones seem to pipe through the hanging wall, but the OCC may still be active since corrugations can be followed almost to the present-day axial valley. A prominent volcanic ridge, >10 km in length, terminates into a characteristic "J" shape at its westernmost end, where it joins the southern end of the Owen Transform Fault.

5.2. The Transform Valley

Figure 7 shows a 230-km-long seismic line running along the axis of the Owen Transform Fault valley parallel to its strike (location in insert map and in Figure 6a). The age of the oceanic basement (all ages estimates quoted in this section use India-Somalia motion of DeMets and Merkouriev (2021)), varies from ~23 Ma to the north to ~7 Ma to the south. Correlatively, the first sediments get younger when approaching the Carlsberg Ridge (Figures 7c and 7d). The total sediment thickness varies from 0.9 sTWTT at the northern gate of the valley (Figure 7a) to >2.6 sTWTT at its deepest point (~4,000 m, Figures 7c and 7d), illustrating the abundant input from the Indus Fan.

R6 (4.3–4.44 Ma) is the oldest calibrated reflector unambiguously identified in the valley until it pinches onto the ~11 Ma oceanic basement. Below R6, the age of the remaining one-third to one-half of the section can only be roughly estimated. Tracking the deeper reflectors found in local depocenters (Figure 7a–7c) would have required a denser network of seismic lines. Close examination of the lines north of the valley indicates that R10 (~8.6 Ma) did not enter the valley, which gives an age limit for the turbidite filling. We cannot rule out that older hemipelagites are present immediately above the basement, but they would have to be thin since the turbiditic facies comes close to the basement in most places. In some other places, chaotic facies is found close to the basement, possibly related to local slope instability.

In the southern half of the line (south of line quoted A in Figure 7c), sedimentary units consistently show a fanning configuration: thickness increases southward until sediments abut the hanging reliefs of Carlsberg Ridge. Wedge thickening affects all layers beneath a well-marked unconformity bracketed between R5 (2.4–2.5 Ma) and R3 (1.1–1.5 Ma) (Figures 7a and 7b), hereafter referred to as D1. The transparent unit immediately above D1 systematically onlaps from the south, and the subsequent series are conformable and more or less constant in thickness.

The entire line displays a rather dense network of buried normal faults (Figure 7), found to be oriented more or less perpendicular to the main axis of the valley, that is, parallel to the oceanic fabric. Half of these ridge parallel normal faults dip toward the Carlsberg Ridge axis, the other half opposite. These faults cut across the sediments down to the basement. An important observation is that a very large proportion of these faults become inactive after D1 (Figures 7a–7c), except at the southern end of the basin (Figures 7c and 7d). Several of these faults seem to have a throw increasing with depth indicating that they may have been active early in the sedimentation history.

5.3. The Central Transpressive Ridge

Figures 8 and 9 present two profiles across the central ridge and the Owen Transform Fault valley, about 100 and 200 km away from the tips of the Sheba and Carlsberg Ridges, respectively (see location in insert map and Figure 6a). The transform fault basin is limited to the east by the basement formed at Carlsberg Ridge which is ~16–18 Ma at this latitude. The basin is abundantly filled with the distal Indus turbiditic sediments carried by conspicuous turbiditic channels, with total sediment thickness reaching about 2.0 sTWTT (~3,000–3,500 m) along its deepest axis (Figures 8 and 9). Growth of the anticlinal ridge on the western side of the valley isolated a narrow corridor on the Somalian side, along the Sheba highs. There, erosion was strong enough to partially erase the western limb of the ridge anticline (Figure 8).

Unconformity D1 previously identified as a major unconformity in the profile parallel to the valley now appears as a major event on these cross lines. Sedimentary units between R5 and D1 are conformable and constant in thickness (in particular within the anticline), denoting the absence of significant tectonic activity before D1. Details of the onlaps geometry onto the eastern limb of the anticline suggest that the uplift related to the fold growth was rather sudden (zoom in Figure 8c). The onset of the transpressive regime is bracketed between R5

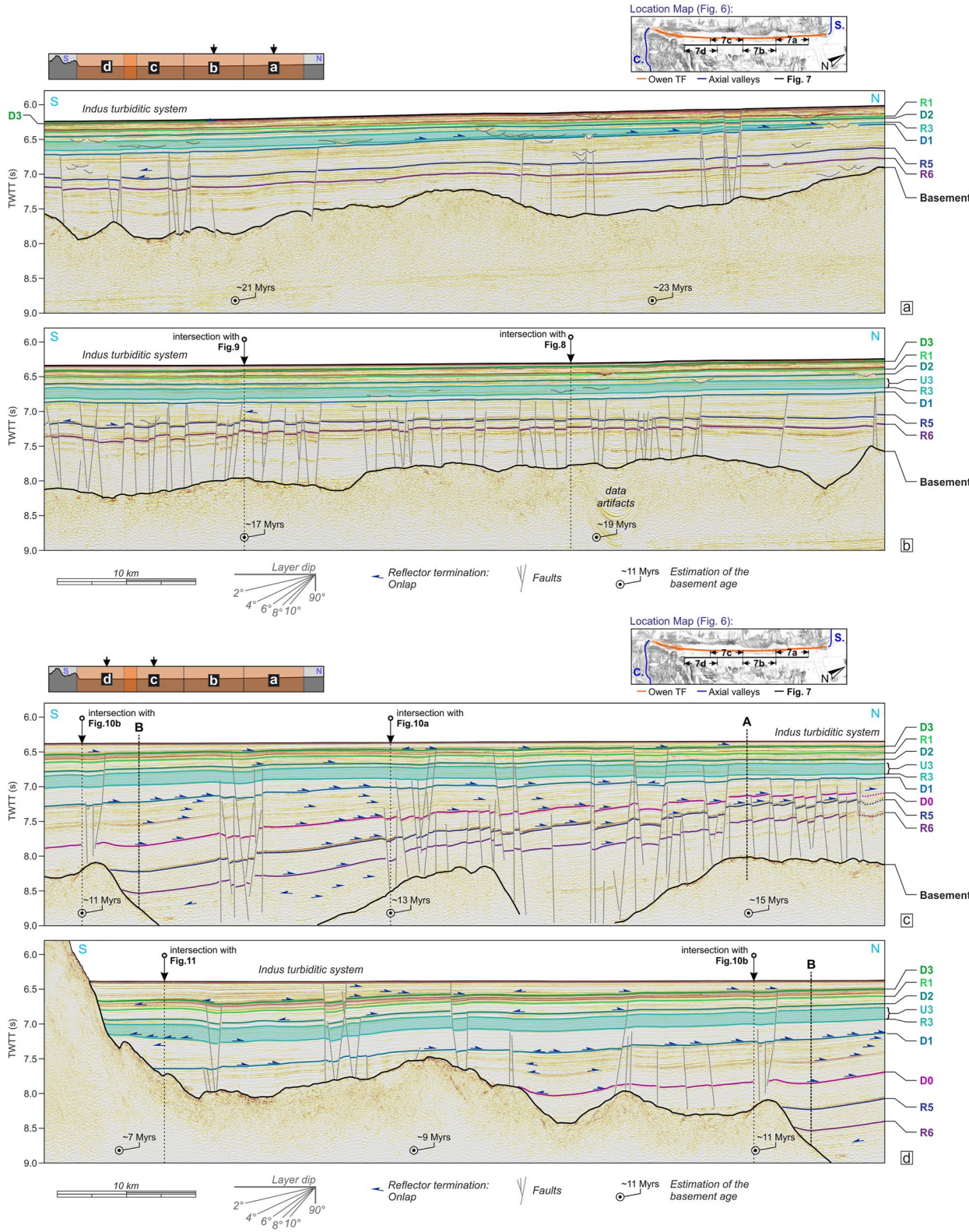

Figure 7. Seismic profile parallel to the Owen Transform Fault valley (location in Figure 6 and in inset map). The overlaying panel shows the relative position of the four sub-figures. The vertical lines indicated by the capital letters "A" and "B" on the sub-figures (c–d) show the portion of the profile where we estimate the finite horizontal extension linked to the normal faulting. Basement ages are estimated using the IN-SM kinematics of DeMets et al. (2020). The entire raw profile is available in Figures S7 and S8 in Supporting Information S1.

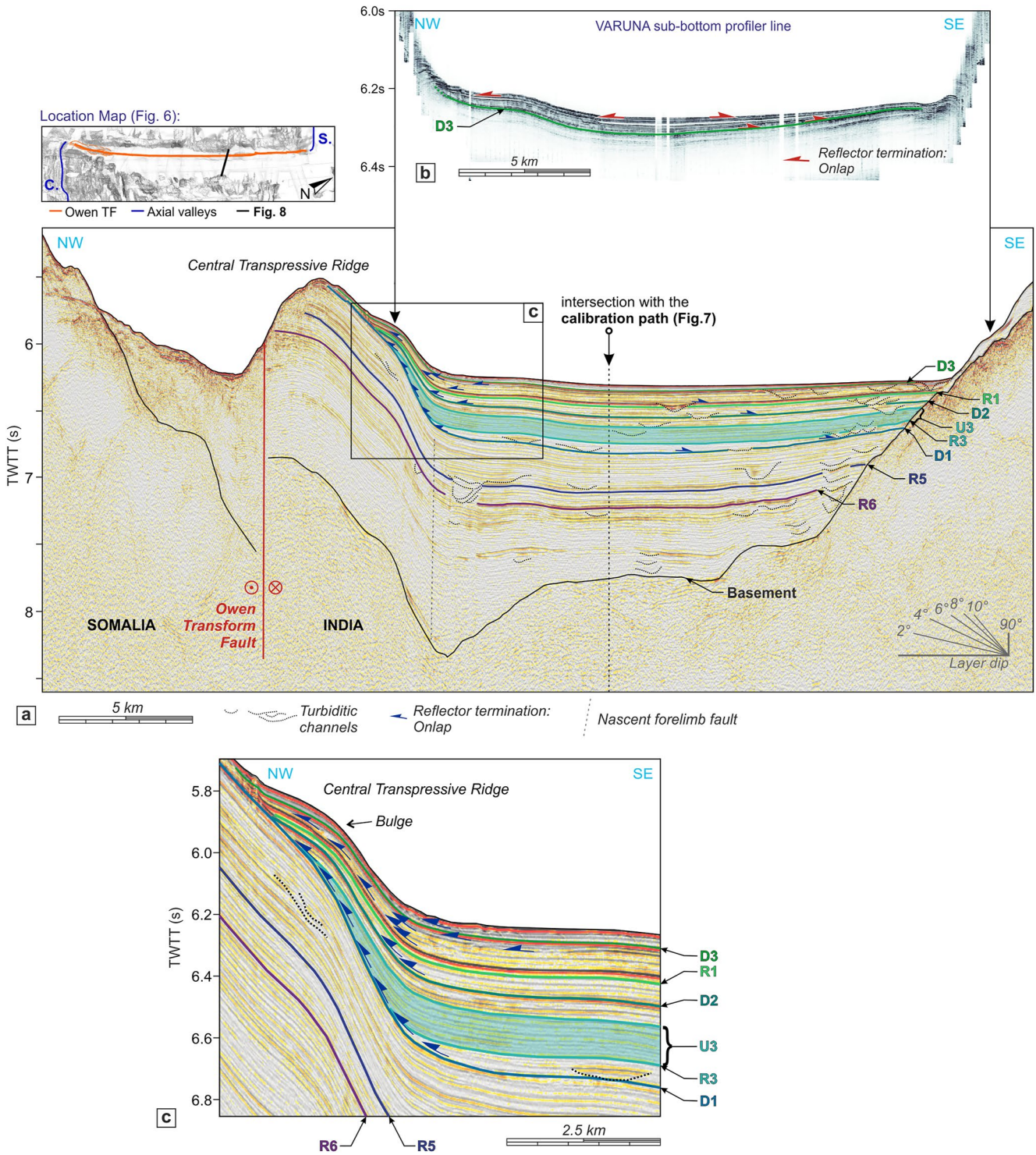

Figure 8. Seismic profile across the central transpressive ridge (location in Figure 6 and in inset map). (a) Interpreted seismic profile. (b) Sub-Bottom Profiler line. Thick black arrows give the position of the sub-bottom profiler line on the seismic line. (c) Zoom on reflectors at the feet of the ridge. The raw profile is available in Figure S9 in Supporting Information S1.

(2.4 Ma) and R3 (1.5 Ma). Secondary unconformities may be present above D1: D2 (0.82–1.10 Ma) between the top of U3 and reflector R1, and D3 (<0.82 Ma) above R1. Both unconformities terminate at an angle with D1 and follow the growth of the central transpressive ridge, forming a wedge-shaped deposit on the eastern limb of the anticline. The pulsated nature of the Indus turbiditic system that fills the transform valley prevents us from

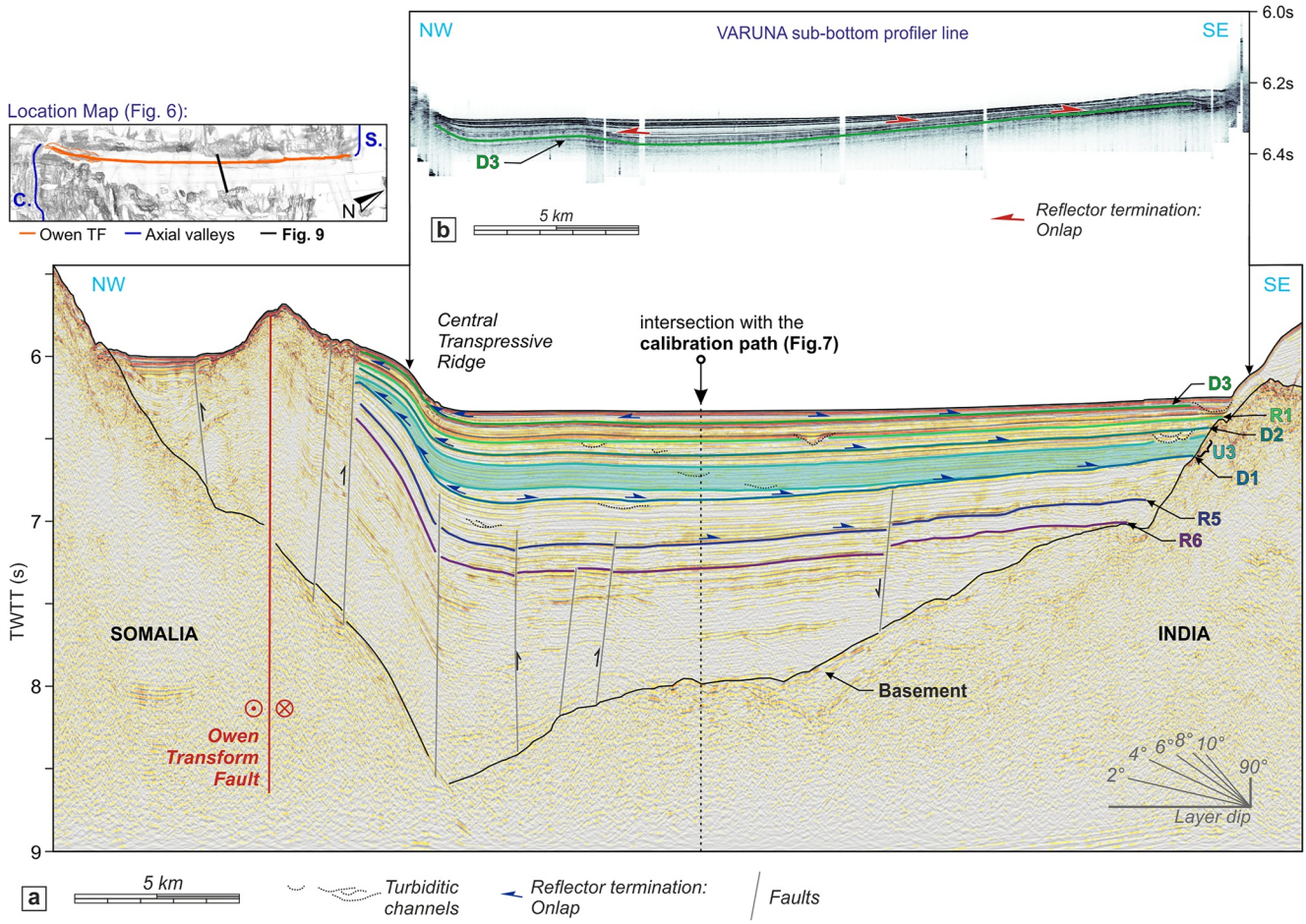

Figure 9. Seismic profile across the central transpressive ridge (location in Figure 6 and in inset map). (a) Interpreted seismic profile. (b) Sub-Bottom Profiler line. Thick black arrows give the position of the sub-bottom profiler line on the seismic line. The raw profile is available in Figure S10 in Supporting Information S1.

clearly distinguishing whether the secondary unconformities above D1 come from a pulsated tectonic regime or the pulsated sedimentary record.

A slight bulge ~30–50 m high is growing at the foot of the ridge anticline (Figure 8c), possibly on an active blind nascent forelimb fault. SBP profiles (Figures 8b and 9b) show further evidence for recent compressive activity accompanying the development of the central ridge en-échelon folds (see location in insert map and Figure 6a). Figure 9b shows that the shallowest sediments are affected, suggesting a continuous growth of the central ridge since D1 (1.5 − 2.4 Ma) or at least D2 (0.82–1.10 Ma) or D3 (<0.82 Ma) up to the recent time. Considering the elevation difference of strata adjacent to the fold in the transform fault valley, the cumulated uplift since the onset of the transpression regime at D1 amounts to ~1.2 sTWTT (~1,250 m) corresponding to an average uplift rate of ~0.5–0.9 mm yr^{-1}.

The normal faults identified on the parallel profile barely show in these cross lines. Only one of them is cut (Figure 9), and de-activated at D1, confirming that these faults are parallel to the oceanic fabric and that their activity stopped at D1.

5.4. The Intermediate Transpressive Region

The intermediate region that runs from the central to the southern ridges is heavily sedimented, both within the transform fault valley and over the adjacent Somalian terrace (seismic profiles in Figures 10a and 10b). Sediment thickness exceeds 3 sTWTT (>5,000 m) in the thickest portion of the transform fault basin, and the basement

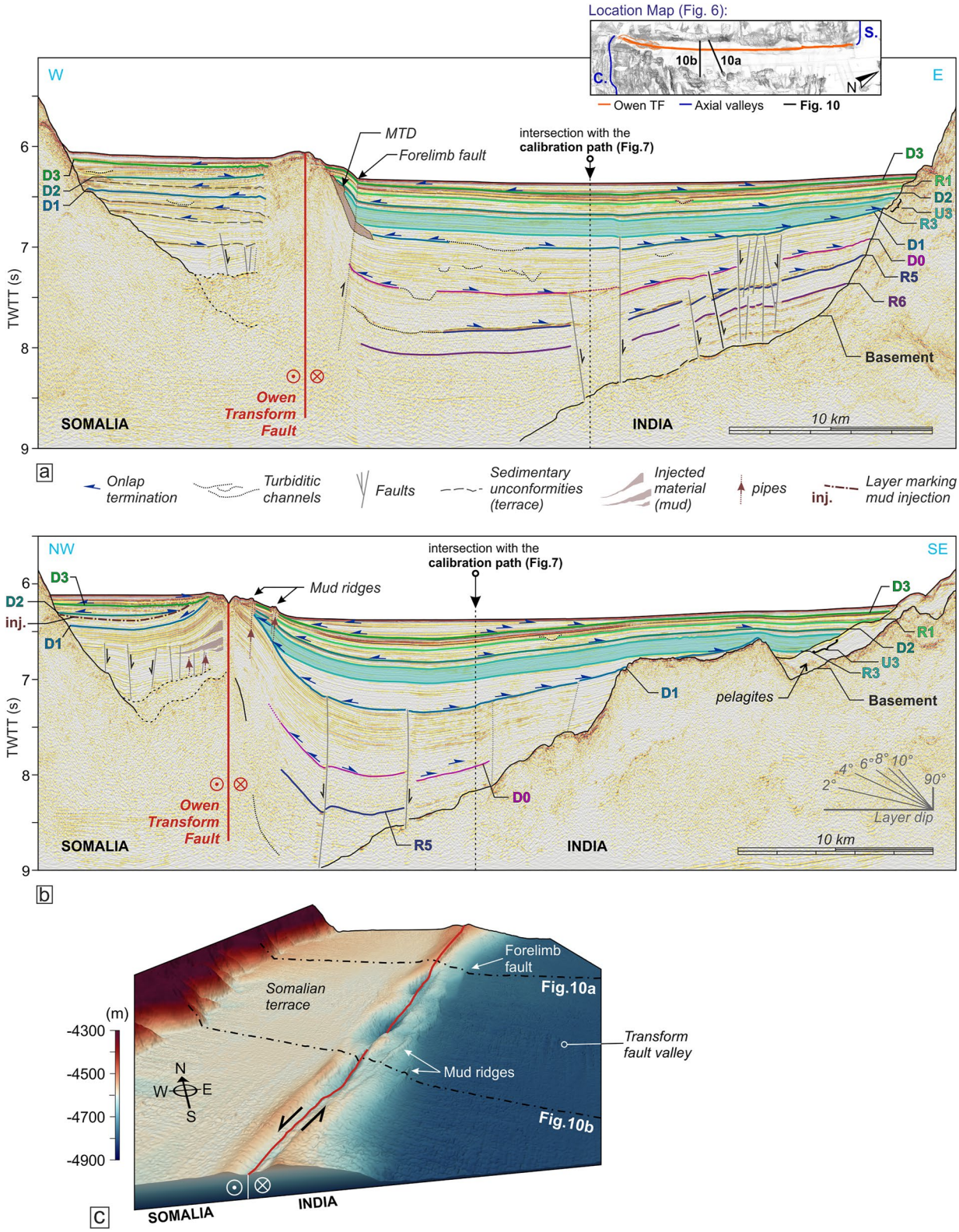

Figure 10. Seismic profiles across the intermediate ridge (location in Figure 6 and in inset map). (a, b) Interpreted seismic profiles. (c) Interpreted 3-D bathymetry (location and orientation in Figure 6). The raw profiles are available in Figure S11 in Supporting Information S1.

is lost below 9 sTWTT in the seismic profiles. The continuous ridge marking the active trace of the Owen Transform Fault is subdued, standing only tens of meters above the Somalian side seafloor. Few fossil turbiditic channels are present, without levees, but their number reduces southward, the overall turbiditic flow of the Indus Fan becoming less and less channelized (compare Figures 8–10). Unconformity D1 is recognized throughout as the main tectonic event. Older discontinuities exist in the deeper portion of the section as discrete onlaps (D0 and R5), but sedimentary units are conformable above and below suggesting little vertical motion.

Sedimentary units recognized within the transform fault basin are only partially identified on the Somalian terrace (Figures 10a and 10b). One sequence beneath D1 (>0.2 sTWTT, Figure 10b) is recognized on both sides, but the correlations below are ambiguous. The youngest units above are also different. Several unconformities absent in the transform fault basin appear in the most recent sedimentary cover on the Somalian side. These observations suggest that sedimentation on the two sides of the transform fault has been temporally disconnected due to the growth of the ridge anticline in between that acted as a barrier. The terrace and the valley seem to have been disconnected since D1.

Two small edifices pop out close to the active fault trace of the transform fault on the Indian plate side (Figure 10b). They closely resemble mud volcanoes in 2-D seismic, but the high-resolution bathymetry (Figure 10c) shows that they belong to two narrow gently curved features that can be followed for more than 5 km, at acute angles to the main fault trace (6° and 11°). Both ridges are connected to pipes that seem to root onto the main unconformities. The ridge closest to the fault is associated with a kink in the entire sedimentary pile. These features are thus interpreted as mud ridges of compressive origin formed in the vicinity of the active fault.

Figure 10b crosses the Owen Transform Fault in an area where its trace on the seafloor is particularly narrow (<1 km) so that both sides display exceptionally well-preserved sedimentary units. Three triangular-shaped units are found in the mid-sedimentary section of the Somalian terrace near the fault (Figure 10b). These units, absent on the Indian side, are characterized by transparent seismic facies unrelated to unconformities. The seismic sequence above shows no change in thickness (about 200 m) while deeper reflectors remain horizontal, implying volume addition in between. Several mechanisms may be responsible for the observed geometry, such as folding onto multiple décollements, channel levees, or bottom current deposits. We favor injection within the core of the fold based on the coarse facies in seismic, the uniform overlying sequence recognized on both sides of the fault, and the evidence for sediment mobilization nearby as mud ridges. The nature of the injected material and its original depth are unknown. The injection event is recorded as a clear unconformity on the Somalian side between D1 and D2 (Figure 10b). Recalling the 20 km/Myr rate on the Owen Transform Fault, the eastern counterpart has been displaced to the north and thus does not show on the profile.

5.5. The Southern Transpressive Ridge

The southern ridge is facing the youngest oceanic basement formed at the Carlsberg Ridge (Figures 6a and 6d). Still wide in the north (>25 km), the transform fault valley narrows down southward (<10 km) where it becomes strictly confined between the transpressive ridge on one side and a prominent inside-corner oceanic core complex on the other side. Sediments transported from the north abut southward on the fresh and not yet subsided Carlsberg reliefs. Progressive infilling of the valley offered sediments routes to the tip of the Carlsberg Ridge only recently.

One seismic profile (Figure 11, see location in insert map and Figure 6) crosses the transform fault valley where the southern transpressive ridge is nascent. At this latitude, the transform fault valley appears as an asymmetric syncline with a maximum sediment thickness of ~2.5 sTWTT (>4,000 m), well-developed above a deep west dipping basement ~6–7 Ma in age. Turbidites, totally unchannelized, are all younger than horizon R5 (2.4–2.5 Ma). The tectonic history is similar to that of the regions further north. Unconformity D1 is found under ~1.3 sTWTT (Figure 11a), highlighted by several onlap terminations and followed by a quiet period in the sedimentary record (0.6 sTWTT). D2 corresponds to a minor unconformity, as was found further north. All sediments above D3 show a conspicuous wedge-shaped configuration related to differential vertical motion between the center of the valley (subsidence) and the shoulder (uplift), as expected for growth strata on a growing fold. The SBP line (Figure 11b) shows the same pattern, indicating that deformation remains active. The locus of the uplift is on the western side of the valley as for the central transpressive ridge, but discrete onlaps are also found on the eastern side. They may relate to a gently growing fold with an east-dipping axial surface.

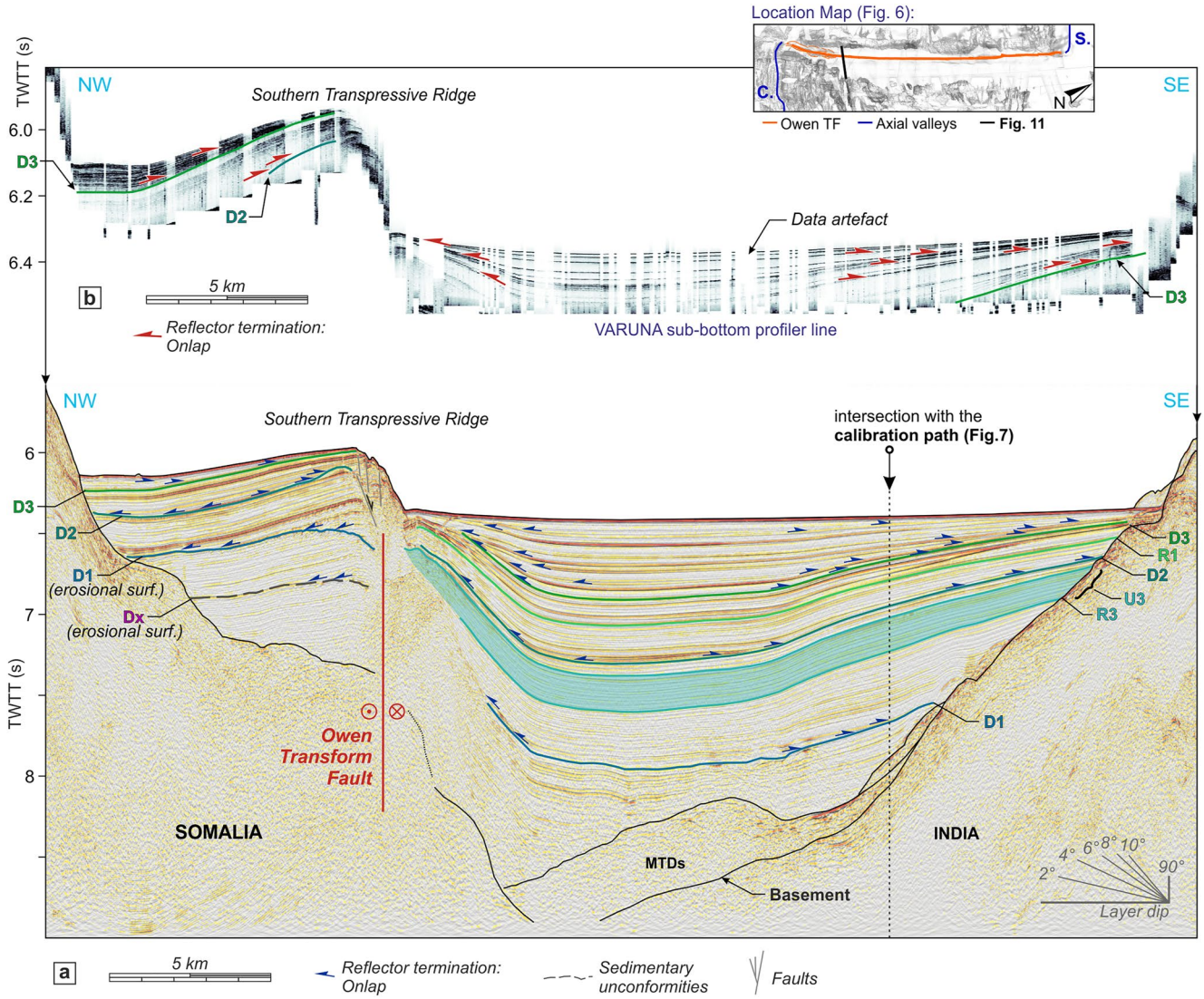

Figure 11. Seismic profiles across the northern part southern transpressive ridge (location in Figure 6 and in inset map). (a) Interpreted seismic profile. (b) Sub-Bottom Profiler line. Thick black arrows give the position of the sub-bottom profiler line on the seismic line. The raw profile is available in Figure S12 in Supporting Information S1.

The sedimentary cover on the Somalian side of the transform fault forms a tilted terrace, whose head makes a sharp bathymetric step (Figure 11). The scarp, several hundreds meters high, now constitutes a barrier delimiting two sedimentary sub-basins that may have been occasionally connected in the past. D3 corresponds to a drastic change of sedimentation on the terrace. The SBP line (Figure 11b) shows that sediments deposited after D3 form a finely stratified, high-amplitude units probably corresponding to pelagites. Two unconformities on the Somalian side are associated with erosional surfaces, corresponding to episodes of abandonment of the turbiditic sedimentation on the terrace. The top erosional surface is identified as D1. The second one is called Dx.

Figure 12 shows a seismic profile that intersects the southern ridge where it culminates more than 1,000 m above the seafloor. The transform fault valley becomes narrow (<10-km-wide) and the seismic basement is shallow and young (~4–5 Ma). The flank of the ridge is steep with slopes commonly >10°. The ridge appears as a tilted oceanic slab. The basement is locally exhumed, hanging ~600 m above the seafloor. The uplifted sediments forming the ridge are similar to those described previously within the terrace, but they are strongly tilted as well as unconformity D1 (compare Figures 11 and 12b). Beneath D1 we recognized Dx, the same erosional surface as in Figure 11, more or less parallel to D1. Thus, the shape of the sediment deposits suggests that severe tilting of the southern ridge initiated at D1 with transpression, uplift, tilt, and change in the type of sedimentation

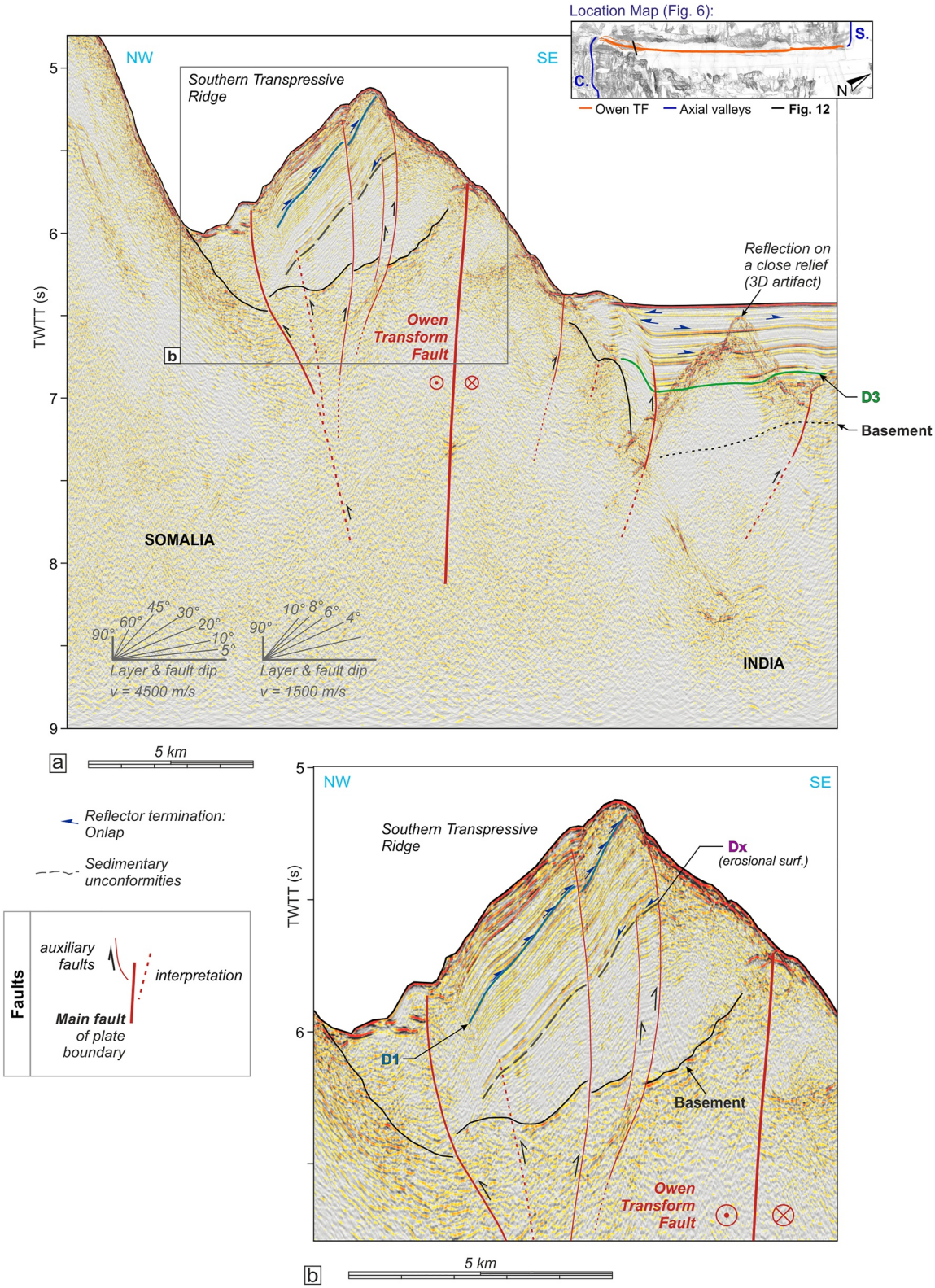

Figure 12. Seismic profiles across the southern transpressive ridge (location in Figure 6 and in inset map). (a) Interpreted seismic profile. (b) Zoom on the tilted sedimentary cover. The raw profile is available in Figure S13 in Supporting Information S1.

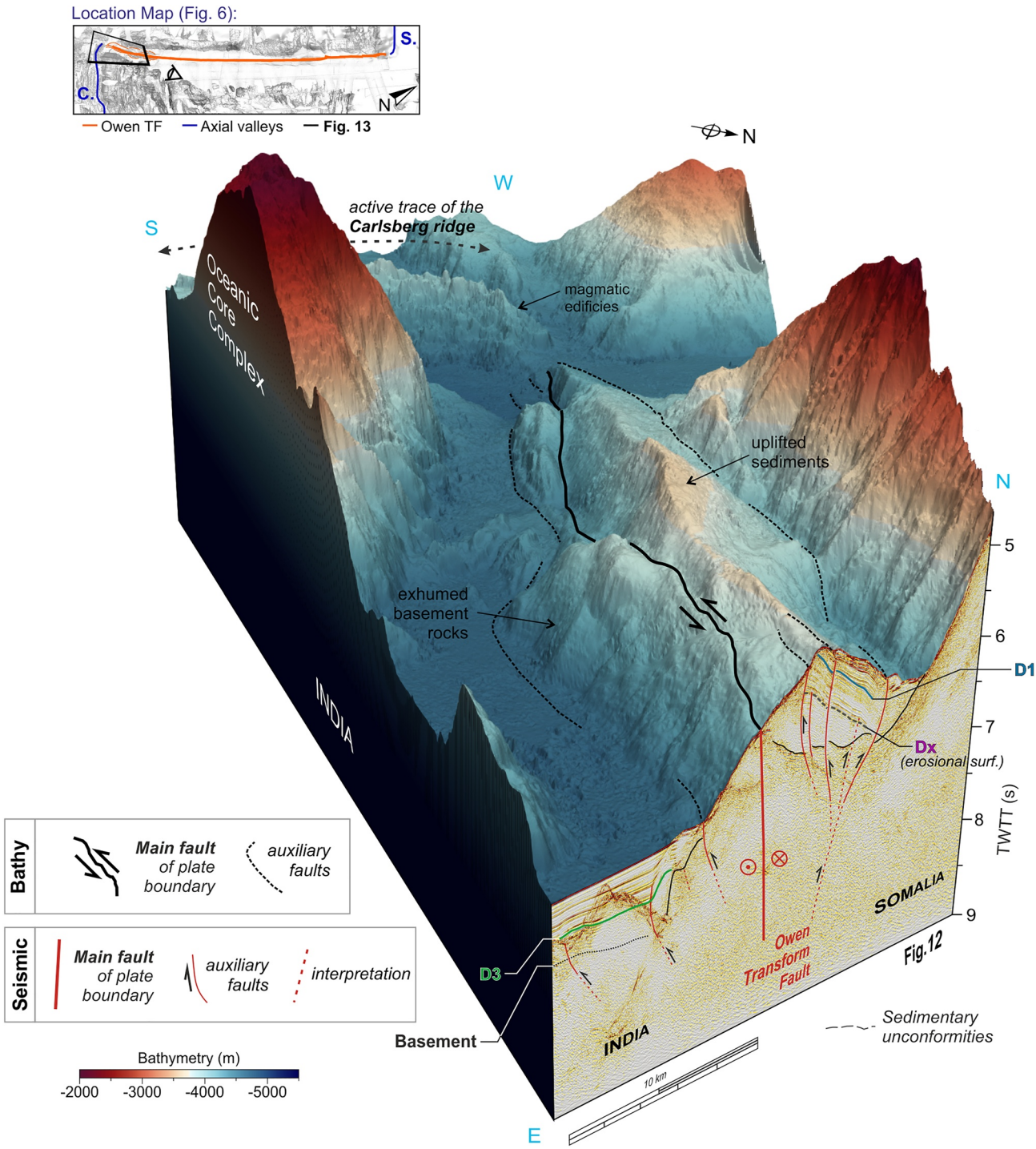

Figure 13. Interpreted 3-D block of the southern ridge looking from the North toward the tip of the Carlsberg Ridge: Seismic profile wrapped with the 3-D multibeam bathymetry acquired during the VARUNA and CARLMAG cruises, location and orientation in Figure 6 and in the insert map.

toward pelagites (<0.1 sTWTT above D1). At the foot of the ridge, unconformity D3 and younger sediments are folded, attesting to active compression. One additional fold is growing in the valley itself, some 5 km away from the main scarp. Taking into account the current bathymetric step and assuming that it is post unconformity D1 (1.5–2.4 Ma), the minimum uplift rate averages to ~0.5–0.7 mm .yr^{-1}.

Figure 13 combines the seismic profile of Figure 12 and the 3-D bathymetry of the entire southern ridge (see location in insert map and Figure 6d) allowing to visualize the spatial evolution of the main structures in three

dimensions. The current morphology of the southern ridge corresponds to a positive flower structure. The fault system is dominated by one main strike-slip fault, well marked on the bathymetry. This main fault is surrounded by secondary thrust faults accommodating the compression.

6. Discussion

6.1. Tectonic History of the Owen Transform Fault and Successive Tectonic Regimes

Figure 14 presents a set of reconstructions of the Owen Transform Fault through time from its early Miocene formation to the present, together with the relevant morphological and tectonic structures. It combines results from the literature for the older periods and the new observations made in this study for the more recent time.

The reconstruction starts with the configuration shortly after the initiation of the Owen Transform Fault. The timing for the establishment of the modern Carlsberg/Owen/Sheba ridge-and-fault system is bracketed between the time of the rapid spread of extension in the Gulf of Aden (~24 Ma, Bosworth et al., 2005) and the oldest oceanic crust (magnetic Chron 6, ~20 Ma, Fournier et al., 2010). Manighetti et al. (1997) argue that the Sheba Ridge nucleated not far from the tip of the Carlsberg Ridge before propagating westward, following a mechanism of dykes propagation within an elastic continental lithosphere (Arabia/Africa) subjected to side slip (India shear) (Hubert-Ferrari et al., 2003; Manighetti et al., 1997). In their scenario, the Sheba Ridge resulted from the propagation of the Carlsberg Ridge toward the Ethiopian hotspot, initiated close to the Carlsberg Ridge tip at some point along the Owen Fracture Zone. However, spreading rates at Sheba and Carlsberg Ridges do not seem to have been very different through the Miocene (since Chron 6), and no significant asymmetry was detected at either ridge, at the level of confidence of the magnetics (Chamot-Rooke & Fournier, 2009). Significant lengthening of the Owen Transform Fault through time is thus improbable.

By contrast, Steckler and ten Brink (1986) propose that the Sheba Ridge initiated far north, away from the tip of the Carlsberg Ridge. Their assumption is that the cold and resistant Late Jurassic to Early Cretaceous North Somali Basin (Cochran, 1988) acted as a lithospheric barrier to straight propagation. A likely hypothesis is that the location of nucleation of the Sheba Ridge along the Owen Fracture Zone occurred at a pre-existing weak point, possibly in the region of Mount Error Guyot and Sharbithat Ridge (Figure 1), which formed a single chain of seamounts before the Gulf of Aden opening (Cochran, 1981; Whitmarsh et al., 1974a). The Owen Transform Fault was thus of very-long offset type from the start, and its length did not change as expected for long transform faults (Stoddard & Stein, 1988). After a short phase of intra-oceanic rifting (Stein & Cochran, 1985), the nascent Sheba Ridge rapidly propagated toward Afar, leaving behind the Owen Transform Fault with its present-day offset.

The next clear tectonic signal recorded in the seismic lines is the uplift of the Owen Ridge around 8.6 Ma (Rodriguez, Chamot-Rooke, Huchon, Fournier, & Delescluse, 2014) along the Owen Fracture Zone (Figure 4). This uplift was coeval with the initiation of the intraplate deformation in the Central Indian Ocean (Bull et al., 2010; Delescluse et al., 2008; Stevens et al., 2020), but the tectonic link is not straightforward. According to DeMets et al. (2020), there was no change in India-Somalia plate motion around this time. However, we note that this time coincides with the beginning of the filling of the Owen Transform valley with the turbidites of the Indus Fan, perhaps due to an increased sedimentary flux over the distal cone or its diversion linked to the uplift of the Owen Ridge to the north (Figure 14b).

The post-8.6 Ma period is the best covered by our study (Figure 14). Based on our calibration and interpretation of the seismic lines in the transform valley, two main tectonic regimes were recorded in the sediments: a phase of diffuse extension re-activating the oceanic fabric perpendicular to the Owen Transform Fault, and a phase of compression that led to the formation of the compressive ridge. The strongest unconformity D1 marks the transition between these two regimes. The normal faults observed within the transform valley (Figure 7) span the entire length of the transform fault and affect the entire pre-D1 units. Furthermore, these faults seem to have been active simultaneously without clear abandonment with the distance to the Carlsberg Ridge axis, at variance with near-axis off-ridge faults of the type documented by off-axis seismicity (Bergman et al., 1984; Pinzón & Vargas, 2021; Tsang-Hin-Sun et al., 2016). A crude estimation of the finite horizontal strain related to this extensional phase leads to modest deformation: summing up individual fault displacements assuming dips of $60 \pm 10°$, the total horizontal strain would be in the range 600–1,200 m between the vertical lines labeled 'A' and 'B' in Figure 7, equivalent to a maximum ~0.5%–1% strain distributed equally between south-dipping and north-dipping normal faults.

Tectonics
10.1029/2023TC007747

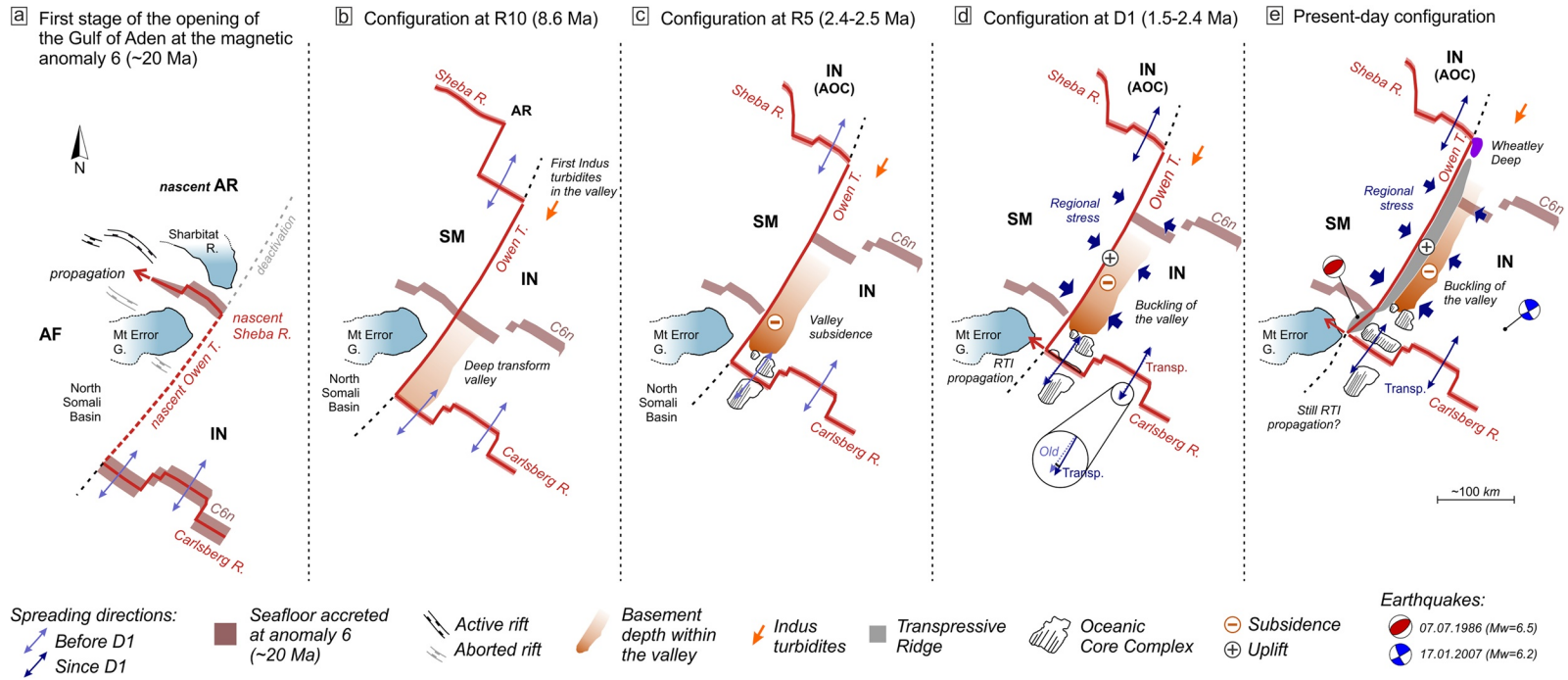

Figure 14. Sketch of the evolution of the Owen Transform Fault since its formation ~20 Ma. The four schematic sub-figures (a-d) illustrate the configuration of the Owen Transform Fault at four key moments. Mount Error Guyot (i.e., Somalia plate) is kept fixed to emphasize the brushing of the Carlsberg Ridge tip along the old North Somali Basin. (a) First stage of opening of the Gulf of Aden following rifting at Sharbitat Ridge and Mount Error Guyot and formation of the Owen Transform Fault (recorded by magnetic Chron 6 (19.7 Ma) at the nascent Sheba Ridge). (b) Configuration of the Owen Transform Fault at R10 (8.6 Myr) during when we suspect the arrival of the first Indus turbidites within the transform valley. (c) Configuration of the Owen Transform Fault at R5 (2.4–2.5 Myr), before the onset of the transpression. At that time, sediments record the subsidence of the southern part of the transform valley. (d) Configuration of the Owen Transform Fault at the onset of the transpression regime (1.5–2.4 Myr), at a time corresponding to the formation of the D1 unconformity in the sedimentary record. (e) Present-day configuration. The two compressive focal mechanisms displayed in (e) illustrate the current stress field in the oceanic lithosphere at two key points: at the southern ridge (red focal mechanism corresponding to the 7 July 1986 earthquake, $Mw = 6.5$) and far from the transform fault (blue focal mechanism corresponding to the 17 January 2007 earthquake, $Mw = 6.2$). AF, Africa; AR, Arabia; IN, India; Owen T., Owen Transform Fault; Mt Error G., Mount Error Guyot; R., Ridge; RTI, Ridge Transform Intersection; SM, Somalia; Transp., Transpression.

We relate these faults to the tectonic regime that prevailed at the transform fault before transpression. At distance from the transform fault, the maximum horizontal stress is expected to be σ_2 compatible with mid-oceanic ridge parallel faulting, switching to σ_1 when approaching the strike-slip zone. Such a stress distribution was found across the Hadibo transfer zone between the western and the eastern part of the Socotra Island (Fournier et al., 2007) or along the aerial segment of the Tjornes Transform zone in Iceland (Angelier et al., 2000). The same pattern is found in numerical models in the case of an uncoupled or weakly coupled transform fault (Behn et al., 2002).

The switch of the tectonic regime from relative quiescence (or moderate extension) to transpression along the Owen Transform Fault took place around 1.5–2.4 Ma (Figure 14). Transpression led to the formation of the continuous anticlinal ridge that runs along the transform fault as well as the overgrowth of the broad syncline adjacent to the fault in the transform fault valley. The onset of compression was coeval with a re-organization of the westernmost accreting segment of the Carlsberg Ridge (Figure 14d). The youngest OCC at the tip of the ridge is exactly facing the southern compressive ridge, suggesting that both features are linked in space and time and related to the same re-organization event. A crude estimate of the age of initiation of this young OCC can be made based on the length of the corrugated surface (Figure 6d). Using the kinematic model of Buck et al. (2005), the heave of the fault L can be expressed as $L = v\tau(1 - M)$ where v is the full spreading rate, τ the age of the OCC and M is the fraction of $v\tau$ accommodated by magmatic dyking. With $L = 21 \pm 3$ km (Figure 6d), $v = 21 \pm 1$ mm . yr^{-1} (see Section 2.1) and M between 0.3 and 0.5 as suggested by observations and modeling at RTIs of slow ridges (Behn & Ito, 2008; MacLeod et al., 2009; Olive et al., 2010), we bracket the age of the OCC at the tip of the Carlsberg Ridge between 1.2 and 2.4 Ma, which overlaps with the timing of the initiation of the transpression.

"J" shaped ridges at the tip of the Carlsberg Ridge are morphologically similar to those described at other transform faults, such as in the southern Atlantic or along the Southwest Indian Ridge (Grevemeyer et al., 2021). The main difference is that the most recent "J"-shaped ridge now connects with the oblique southernmost segment of the Owen Transform Fault, suggesting an effective propagation mechanism into the Somalian plate.

6.2. The Owen Transform Fault and India-Somalia Kinematics

We test in Figure 15 the alignment of the active Owen Transform Fault with the small circles predicted by the India-Somalia recent kinematics, using an oblique Mercator projection whose axis is the Euler pole of rotation that best fits the active fault trace. Several kinematic solutions are available: India-Somalia in MORVEL global plate model (DeMets et al., 2010), India-Somalia best-fitting finite rotations obtained solely from magnetics and transform faults at Carlsberg and northern Central Indian ridges, with or without noise reduction (DeMets et al., 2020), and a revised version of India-Somalia best-fitting rotations (DeMets & Merkouriev, 2021). Two-plate best-fitting models best match the trace of the active fault. Among these models, the latest solution for Chron 1n (0.773 Ma, DeMets and Merkouriev, 2021) and finite noise-reduced rotations for the last 3.6 Ma (DeMets et al., 2020) are indistinguishable. They all predict pure strike-slip on the fault. Also shown in Figure 15 are the small circles derived from India-Somalia in MORVEL: they deviate by 2.3° counter-clockwise from the fault trace and predict a component of compression along the entire length of the fault. The simplest interpretation for Chron 1n kinematics being different than MORVEL is that closure imposed in global plate circuits slightly degrades India-Somalia kinematics. The alternative would be a systematic bias affecting the two-plate reconstructions, which seems unlikely. MORVEL includes only 133 spreading rates and 2 transform fault azimuths measured at the Owen Transform Fault (DeMets et al., 2010), while 1n reconstruction in DeMets and Merkouriev (2021) is based on 337 magnetic chron pickings and 99 transform faults azimuths, suggesting that the latter is better constrained.

Brute (i.e., non-noise-reduced) rotations for the past 10 Ma predict erratic changes in the direction of motion incompatible with our observations: the predicted India-Somalia stage plate slip direction estimated at the Owen Transform Fault is oscillating between −8° and +8° around the mean value from one chron to the other with no systematic trend (DeMets & Merkouriev, 2021). Such drastic switches from transtension to transpression are not observed in seismic profiles, or recorded by striations on the oceanic core complexes. The difficulty in recovering reliable azimuths is related to the noise level inherent to the picking process of the magnetic lineations and associated transform faults. As suspected in DeMets et al. (2020), stage poles derived from magnetic-based reconstruction poles are unstable despite the high number of data used in the latest determination (DeMets & Merkouriev, 2021). Smoothing may be a viable solution for noise attenuation (e.g., Iaffaldano et al., 2012, 2014), but at the expense of erasing the effective fluctuations we are looking for. The difficulty faced here is that minor changes in plate motion produce no more than a few degrees of obliquity, ultimately lost in the noise. Slow-spreading ridges are particularly affected.

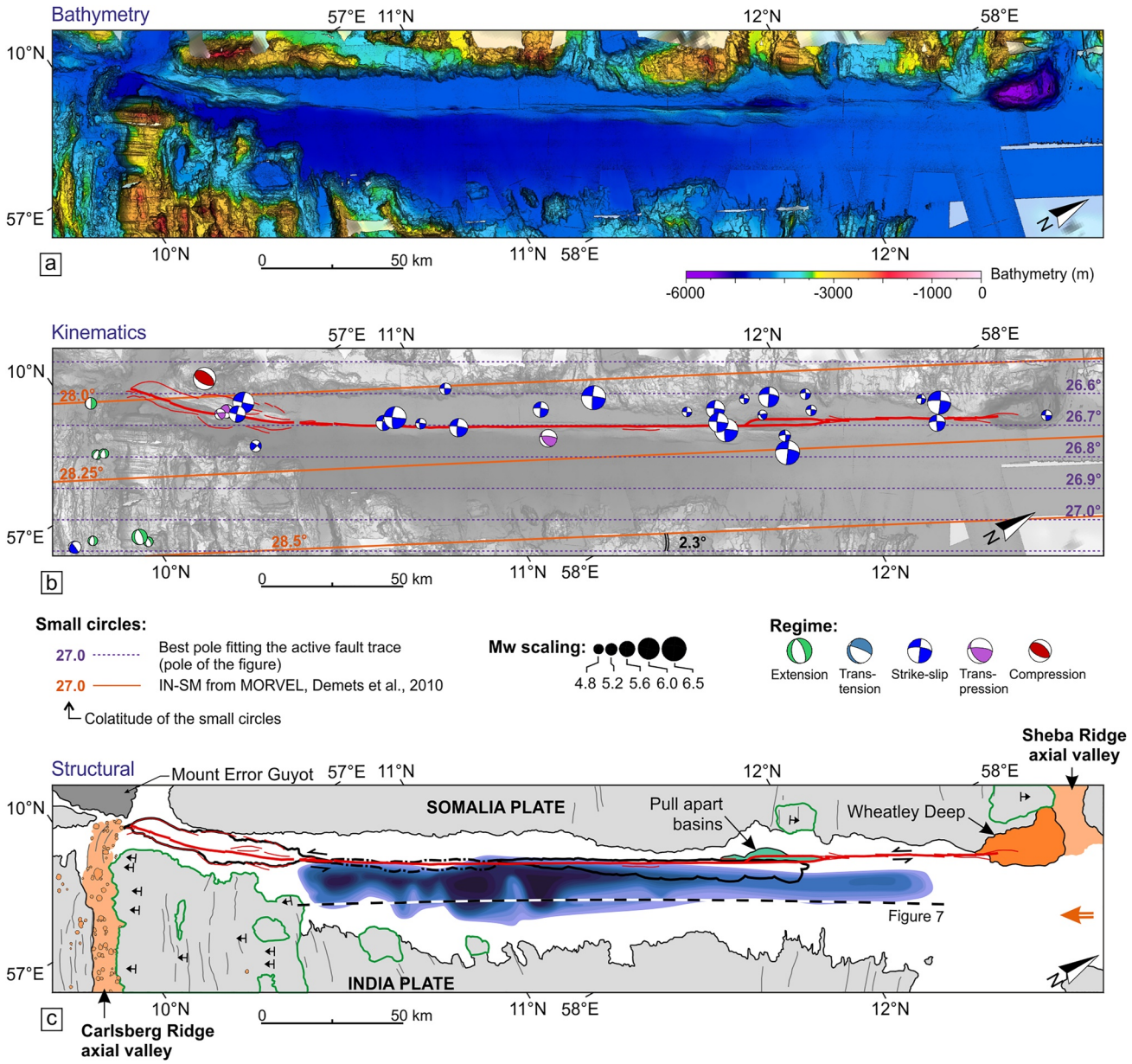

Figure 15.

A remarkable observation is that the fault trace follows the same small circle (within 2 km) for almost 250 km (excluding the southernmost 60 km, Figure 15b). Along most of its length, the present-day surface fault trace is thus conforming to the curvature predicted by the position of the pole, that is, a ∼4° clockwise azimuthal rotation from the northern RTI to the southern RTI. Along its northern portion, the fault trace is left-stepping (2–3 km) forming an elongated pull-apart basin. The overall geometry suggests a minor component of compression there, favoring a close to pure strike-slip motion for the present-day. Further south, many focal mechanisms indicate pure strike-slip, but a small number of them, mostly located over the southern portion of the transform fault, show a compressive component (Figure 15b). One of the strongest earthquakes recorded so far at the Owen Transform Fault (7 July 1986, $Mw = 6.5$) shows a pure thrust focal mechanism, recognized as a puzzling event in early worldwide seismological studies on oceanic transform faults (Wolfe et al., 1993, Figures 14d and 15b). This event occurred onto the main reverse fault of the southern compressive ridge, where departure from pure strike-slip becomes exceptionally large (∼17° clockwise). The fault trace becomes incompatible with a single small circle around the India-Somalia pole, indicating that the RTI departs from rigid two-plate kinematics, as found in several numerical models (Grevemeyer et al., 2021; Mishra & Gordon, 2016). Notice that the extremely high obliquity reached there would imply a dramatic uplift rate of several km.Myr^{-1} assuming two-plate kinematics, a situation that cannot be stable in time.

6.3. Origin of the Transpression on the Owen Transform Fault

Many transform faults and fracture zones show evidence of vertical tectonics (Bonatti, 1978). Departure from a simple strike-slip morphology includes the formation of transverse structures within the transform valley, changes in the strike of the transform faults, and reorganization of the ridge-transform system at the RTIs. Several mechanisms, summarized in Maia (2019) and Marjanović et al. (2020), have been invoked to explain abnormal reliefs at transform faults. These include: serpentine diapirism (Bonatti, 1976, 1978), volcanic injection (Thompson & Melson, 1972), horizontal thermal contraction (Collette, 1974; Kumar & Gordon, 2009; Mishra & Gordon, 2016), differential subsidence (Parmentier & Haxby, 1986; Sandwell & Schubert, 1982; Wessel & Haxby, 1990), and plate motion change (e.g., Menard & Atwater, 1969; Bonatti, 1978; Pockalny et al., 1997). Some of these mechanisms predict distributed extension within the transform valley with transform-parallel faulting (Mishra & Gordon, 2016) at odd with the Owen Transform fault network, which shows predominantly transpression. Differential subsidence due to age contrast at the transform fault may imply an uplift of the young side, producing a symmetrical effect with respect to the center of the fault, maximum at the RTIs and null halfway. Such an age-controlled mechanism is difficult to reconcile with the continuous transpressive ridge observed along the entire length of the Owen Transform Fault, recalling further that the basement topography is not conforming to the expected age symmetry. Bonatti (1976) and then Bonatti (1978) proposed that due to density contrast between the serpentine coming from the hydrothermal alteration of upper mantle peridotites and the unaltered rocks, serpentine could form diapirs and thus produce vertical tectonics. Rocks sampled at transform faults suggest that these faults are places of intense hydrothermal circulation (Kohli et al., 2021; Kohli & Warren, 2020; Prigent et al., 2020) and thus could potentially host serpentine diapirism. However, our seismic profiles show no clear evidence of serpentine intrusion and ductile deformation. Moreover, if true, this hypothesis required in our case the formation of a localized and continuous intrusion all along the Owen Transform fault as well as a none steady-state dynamics to explain the formation of the D1 unconformity. Finally, volcanism close to the transform fault is absent from our seismic lines. Magmatism seems to have been restricted to the axes of the mid-oceanic ridges, with no off-axis contribution.

In most cases, vertical tectonics at transform faults have been attributed to plate kinematic changes (e.g., Bonatti, 1978; Bonatti et al., 1994; Maia, 2019; Maia et al., 2016; Marjanović et al., 2020; McCarthy et al., 1996; Pockalny, 1997; Pockalny et al., 1996, 1997; Tucholke & Schouten, 1988).

Among the best-studied cases of transform faults where compression followed a plate motion change are those of Kane in the northern Atlantic Ocean (Pockalny et al., 1996; Tucholke & Schouten, 1988), Romanche (Bonatti

Figure 15. Graphical test of the alignment of the Owen Transform Fault with India-Somalia small circles. Subfigures (a–c) are Oblique Mercator projections using a rotation pole that best fit the active trace of the Owen Transform Fault (lat = 23.25°N, lon = 32.50°E; mean pole of DeMets et al. (2020) for the last 2 Myr). (a) Bathymetric map of the Owen Transform Fault and surroundings from the tip of the Sheba Ridge to the tip of the Carlsberg Ridge. (b) Sismo-kinematic panel showing the surface fault trace of the Owen transform (in red), Focal mechanisms are colored according to the tectonic regime. Small circles of our rotation pole are horizontal lines (in purple). The plain orange lines are the MORVEL (DeMets et al., 2010) IN-SM small circles. Focal mechanisms are Global Centroid-Moment-Tensor project solutions (GCMT, Dziewonski et al., 1981; Ekström et al., 2012) published in the International Seismological Centre (ISC) Bulletin and re-localized using the Event catalog of the ISC (International Seismological Centre, 2021; Storchak et al., 2017, 2020). (c) Structural map of the Owen Transform Fault vicinity. The filled contours represent the depocentre model of the Owen Transform Fault valley (sediments cover >∼1.5 sTWTT) estimated from seismic profiles picking.

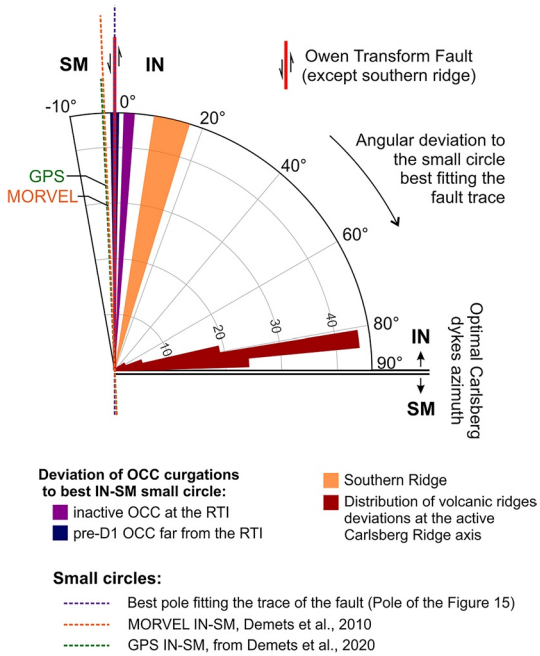

Figure 16. Rose diagram showing the angular deviation of several structures and kinematics to the small circle best fitting the active trace of the Owen Transform Fault (pole of Figure 15). In this projection, the vertical is the local strike of the Owen Transform Fault (red line). The horizontal corresponds to the predicted Carlsberg dikes azimuth (black double line).

et al., 1994) and Saint Paul (Maia et al., 2016) in the Equatorial Atlantic Ocean and Clipperton along the East Pacific Rise between the Pacific and the Cocos plates (Pockalny, 1997; Pockalny et al., 1997). In the Equatorial Atlantic, the kinematic change responsible for the compressive tectonics observed at Vema, Saint Paul, and Romanche transform faults seems to have occurred around 10–11 Ma (Bonatti et al., 1994, 2005; Maia et al., 2016) in response to a slight change in the direction of Nubia-South America plate motion. This interpretation was partly challenged by findings at the 300-km-long Chain Transform Fault located south of the Romanche fault (Harmon et al., 2018, and discussion in Marjanović et al., 2020). Detailed mapping and magnetic interpretation showed that the positive flower structures found locally along the Chain Transform Fault initiated at different ages and affected only a portion of the fault, suggesting that they cannot be related to a single 10–11 Ma event. Harmon et al. (2018) propose instead that fluctuations in the magmatic input on both sides of the transform fault, accompanied by RTI propagation and retreat, forced local segment-scale re-organization and transient stress changes at the origin of the complex morphology.

Kinematic changes are likely to be recorded not only along the transform faults themselves but also at the nearby accretionary ridge segments. Changes in the strike (rotation), length, and height of the abyssal hills along the Pacific-Antarctica Ridge (Cande et al., 1995; Croon et al., 2010; Macario et al., 1994), the Southeastern Indian Ridge (Goff et al., 1997) or along the East-Pacific Rise (Pockalny, 1997; Sonder & Pockalny, 1999) have been interpreted as further evidence for past kinematic changes.

Figure 16 gathers the deviation in volcanic ridges and OCC corrugations orientation at the Carlsberg Ridge (measured in the bathymetry) to the small circle that best fits the Owen Transform Fault. The present-day dyke-perpendicular orientation (<1 Ma) measured along the Carlsberg Ridge axis up to 200 km away from the Owen Transform Fault systematically deviates counter-clockwise, thus predicting compression on the Owen Transform Fault assuming orthogonal spreading. Corrugations at pre-D1 OCCs align with the fault, suggesting that the Owen Transform Fault did not change in azimuth in recent times. Corrugations of the large westernmost OCC facing the southern ridge (Figure 6d) are slightly clockwise compared to other OCC (Figure 16). However, due to the large clockwise bend of the Owen Transform Fault at its southern end, these corrugations are still compatible with transpression onto the Owen Transform Fault.

A test for an India-Somalia kinematic change would be to seek additional evidence for changes in the tectonic regime at other transform faults offsetting segments of the Carlsberg ridge. Transform faults east of the Owen Transform Fault are all right-stepping so that a counter-clockwise rotation of India-Somalia motion would lead to transpression. However, they are all of short-offset type (<40 km) and thus not prone to large-scale deformation. Yet, one off-ridge intraplate earthquake (17 January 2007, $Mw = 6.2$) attests to the present-day regional compressive stress within the India plate close to the southern RTI (Figure 14e). The event occurred 180 km southeast of the Owen Transform Fault and 120 km northeast of the closest segment of the Carlsberg Ridge. The focal mechanism is pure strike-slip, and the epicenter is close to a fracture zone, but none of the two nodal planes is parallel to it (GCMT solution). The proposed depth (13–23 km quoted in the ISC event catalog according to the various moment tensor solutions) suggests a mantle event. Possible origins of similar intraplate off-ridge events have been discussed by Bergman et al. (1984) and more specifically in Wolfe et al. (1993) for those earthquakes that are close to large transform faults. The proposed causes include abnormal stress state in the lithosphere due to thermal, bending, or volcanic stresses (Bergman et al., 1984), possibly linked to deeper processes at mantle depth such as anomalies in the convection pattern (Harmon et al., 2020). Wolfe et al. (1993) speculate that changes in plate motion are responsible for many of the anomalous earthquakes close to large transform faults, but they acknowledge that additional constraints are needed to support this hypothesis. The P-axis of the 17 January 2007 earthquake is perpendicular to the general trend of the Carlsberg ridge transform faults, the simplest interpretation being that the present-day far-field stress within the Indian lithosphere is compressive not only at the Owen Transform Fault but at some distance from it.

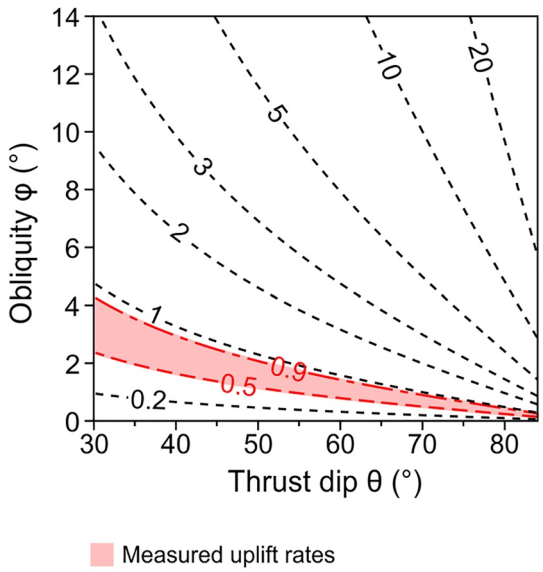

Figure 17. Simple model of uplift rate expected for a thrust dip (θ) and an obliquity (ϕ, counted here counter-clockwise) to an ideal India-Somalia motion.

Taken altogether, these observations are compatible with some amount of oblique motion onto the Owen Transform Fault resulting from a recent counter-clockwise rotation of the spreading direction at the Carlsberg Ridge: (a) transpression affected the entire length of the Owen Transform Fault, (b) deformation initiated suddenly (recorded by a unique seismic reflector all along the fault) following a long period of tectonic quiescence, (c) it was coeval with a re-organization of the Carlsberg Ridge including the westward propagation of its tip into the Somalia plate, and the coeval formation of the southern transpressive ridge and associated OCC at the RTI. By analogy with the well-studied examples of oceanic transform faults displaying transpressive structure we discussed above, it appears that a kinematic change is the most plausible mechanism able to explain both the rapid onset of transpression along the entire length of a transform fault (especially for a long-offset transform fault as Owen) and the simultaneous reorganization of the accretionary system. Transpressive deformation along the Owen Transform Fault may be representative of the first step of formation of a median ridge as described along the Clipperton Transform Fault (Pockalny, 1997; Pockalny et al., 1997) or along the Kane Transform Fault (Pockalny et al., 1988).

6.4. Amplitude and Accommodation of the Compressive Component

Transpression onto the Owen Transform Fault is resolved through a simple strain partitioning process. The main fault accommodates pure strike-slip motion, while the compressive component is accommodated east of the transform fault (Arabian Sea side) by a secondary system of folds (Figures 8 and 9) and reverse faults (Figures 12 and 13). Similar partitioning under a transpressive regime is described over the central part of the Queen Charlotte fault delimiting the North America plate from the Pacific plate (Tréhu et al., 2015). Analytical developments (Fossen & Tikoff, 1993, 1998) based on analogue strain experiments show that this type of simple shear partitioning occurs when the relative plate motion obliquity to the ideal strike-slip is smaller than a threshold of 20°. Braun and Beaumont (1995) reach similar threshold angles of 15–25° using numerical modeling. Deformation observed along most of the Owen Transform Fault is simple shear dominated, compatible with a small angle of imposed oblique motion.

The average uplift rate estimated from the seismic lines since the onset of the transpression is ~0.5–0.9 mm yr^{-1} puts some constraints on the amount of obliquity. Uplift rate (U) can be modeled as a function of the dip of the thrust accommodating the convergence component of the displacement (θ) and the obliquity to an ideal strike-slip motion (ϕ, deviation to optimal IN-SM small circle). Then, $U = v\sin(\phi)\tan(\theta)$ where v is the full ridge normal opening rate at the Carlsberg Ridge. Figure 17 shows that no more than one to four degrees of obliquity (averaged since D1) is required to explain the observed deformation, the most plausible being the lower end since a larger obliquity would invalidate India-Somalia kinematics obtained from global models, for which there is independent support based on the orientation of the striations of corrugated surfaces at Carlsberg oceanic core complexes.

Similar small degrees of obliquity have been quoted at other transform faults as responsible for abnormal morphology. On the mid-Atlantic Ridge, the left-stepping Kane Transform Fault readjusted its strike following a 4°–6° clockwise spreading direction change around 8 Ma, resulting in the formation of a compressional >500-m-high median ridge within the active transform and the simultaneous exhumation in extension of a 40-km-long 1-km-high transverse ridge along its inactive portion, the Kane Fracture Zone (Pockalny et al., 1996). This example shows that modest amounts of obliquity (a few degrees) are enough to produce vertical tectonics both within the transform fault valley and at the inactive fracture zone, even at low spreading rates. In the case of the Kane Transform Fault, the transient period of re-adjustment to the new kinematic conditions lasted several millions of years between 8 and 3 Ma, long enough to build significant reliefs.

6.5. Origin of the Owen Transform Valley

Several non-mutually exclusive mechanisms may explain the formation of the deep Owen Transform valley, such as flexure at the Owen Fault, amagmatic accretion, thinning of the crust, and sediment loading. The Owen

Transform is strongly asymmetric, with a deep valley on the Indian side (oceanic crust formed at Carlsberg Ridge) and hanging highs on the Somalian side (oceanic crust formed at Sheba Ridge). Similar asymmetry has been found at the Romanche Transform Fault, with a magmatic crust on one side and a poorly-magmatic crust on the other side (Gregory et al., 2021). A striking implication of this asymmetry is that the differential topography does not revert halfway between the Sheba and the Carlsberg ridges, at variance with theoretical cooling-with-age predictions and observations at conventional oceanic transform faults: the basement remains deep on the Indian side, even close to the tip of the Carlsberg Ridge. Abnormal subsidence is related to the proximity with the Owen Transform Fault: far from the fault, the basement depth follows a typical plate cooling model (Stein & Stein, 1992) both on the Sheba and the Carlsberg sides (Figure 18a). Figure 18c shows the unloaded basement depth within the transform valley using the valley-parallel seismic line (Figure 7) and assuming local isostasy (details in Text S4 in Supporting Information S1). Near the northern end of the valley, where the oceanic crust predates the formation of the Owen Transform Fault, the unloaded basement reaches more or less the depth predicted by the cooling profile. Within the transform valley, the unloaded basement depth varies between 5,200 and 6,500 m, up to 2,500 m below the expected thermal depth. This abnormal depth is comparable to the current seafloor depth at the Wheatley Deep nodal basin at the eastern tip of the Sheba Ridge, and generally to the depth of other nodal basins (e.g., >5,500 m depth at the RTIs of the Kane Transform Fault (Tucholke & Schouten, 1988), or 6,480 m at the southern nodal basin of the Atlantis II Transform Fault (Southwest Indian Ridge, Dick, 1991)). A possible interpretation is that the oceanic crust is missing (or particularly thin) on the Indian side close to the Owen Transform Fault.

The most likely interpretation for a deep basement is that accretion at Carlsberg is mainly amagmatic, in agreement with the high number of oceanic core complexes flooring the Indian side. The cold environment at the tip of the Carlsberg Ridge may relate to the specific history of the Owen Transform Fault: the southern RTI remained in contact with the cold Late Jurassic to Early Cretaceous North Somali Basin (Cochran, 1988) until the ridge recently reached the latitude of Mount Error Guyot (Figure 14a, see discussion Section 6.1). The northern RTI followed a different thermal path since it has always faced the Eocene Arabian oceanic lithosphere. Thermal asymmetry thus remained throughout the entire history of the Owen Transform Fault.

Grevemeyer et al. (2021) propose a more general and systematic scenario for the formation of the transform fault valley. They observed that the transform fault valleys are always deeper than their fracture zones, independently of their offset or local spreading rate. The anomalous depth may thus be an intrinsic property. Based on a thermo-mechanical model, they propose that the valley is a wide zone of steady-state transtension, crustal thinning, and normal faulting accommodating oblique shearing at depth. This model does not seem to apply to the Owen Transform Fault, since no such shearing is observed in the post 8.6 Ma sediments that fill the valley. The off-ridge normal fault network that we observe before transpression (Figure 7) corresponds to a modest re-activation that cannot be responsible for any significant thinning and correlative deepening of the basement (see discussion Section 6.1).

Since infilling with the Indus-derived turbidites (post 8.6 Ma), the evolution of the subsidence and accommodation space in the valley involves several interacting mechanisms: the basement formed at the Carlsberg Ridge subsides as it moves north toward the entry of the valley, and at the same time sediments enter from the north and down-flex the basement (Figure 15a). Neuharth et al. (2021) described the interesting case of flexural strike-slip basins developing parallel to active strike-slip faults in the case of asymmetrical sedimentation forcing one side of the fault to subside. Their numerical model shows that decoupling of the lithosphere at the strike-slip fault maintains accommodation space at the footwall of the fault allowing the growth of a several-kilometers-thick basin. This model ideally applies to the Owen Transform Fault valley, infilling by the Indus-derived sediments remaining confined to the Indian plate side since the uplift of the Owen Ridge.

7. Conclusions

In this study, we unveiled the present-day morphology and the recent tectonic history of the Owen Transform Fault, sedimented under the distal Indus Fan system. Our results are summarized in the following key points:

- A revisited stratigraphic framework based on seismic and drillings allows us to time-calibrate seismic horizons over the distal Indus Fan. The sedimentary cover is mainly Miocene over a Paleocene basement, with little evidence of a significant volume of Paleogene turbidites, late Oligocene if any. At the entry of the Owen Transform valley, the turbititic sedimentary cover is 8.6 Ma. The most recent turbiditic sediments of the Indus Fan reach the Carlsberg Ridge close to its intersection with the Owen Transform Fault and beyond, routing into the narrow transform fault valley.

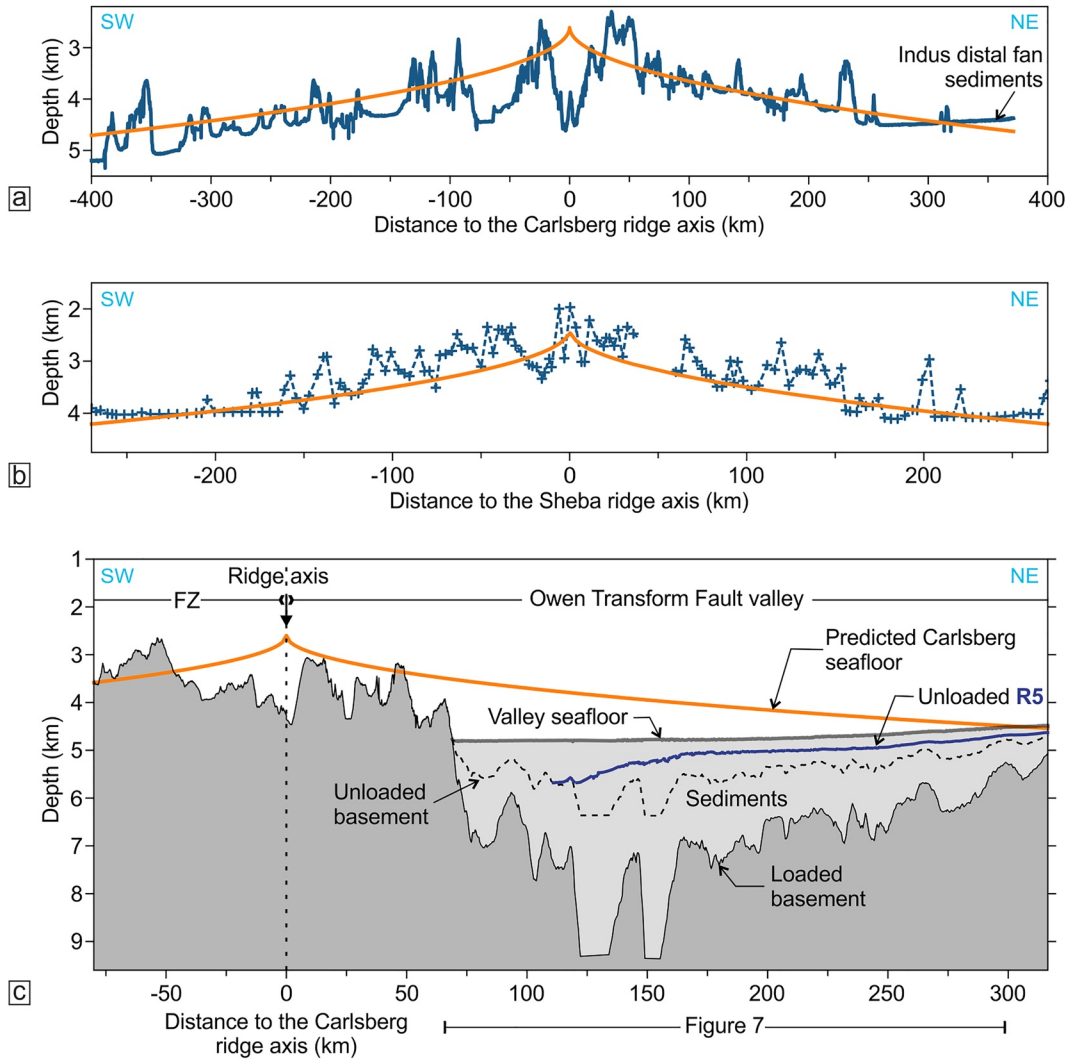

Figure 18. Basement topography and subsidence. (a) Bathymetric profile across the Carlsberg Ridge (blue line), taken along a MORVEL small circle outside of the Owen Transform Fault valley, ~50 km away from the active fault trace. (b) Bathymetric profile across the Sheba Ridge (blue line) crossing the ridge near (56.53°E, 14.36°N). Cruise bathymetric data from the GeoMapApp compilation of Ryan et al. (2009) (profile reference: 19920021). (c) Bathymetry and basement depth within the Owen Transform Fault valley (basement from seismic the profile of Figure 7). Dashed line profile: sediments unloaded basement assuming a local isostasy. The blue line the unloaded reflector R5 (2.4–2.5 Ma). The orange lines in (a-c) are model fits assuming a half-space cooling model following Stein and Stein (1992) (details in Text S5 in Supporting Information S1). The light gray surface represent the sediments cover along Figure 7 seismic profile.

- The Owen Transform Fault shows as a sharp trace in the multibeam bathymetry bounded by a narrow terrace to the west (Somalian side) and a 30-km-wide 300-km-long flexural basin to the east (Indian side) abundantly fed by the Indus-derived turbiditic sediments. A continuous ridge, showing as a broad anticline in seismic, delimits a bathymetric step between India and Somalia. Based on the identification of active features (en-échelon folds, active fault trace, anticline and syncline growth, mud ridges), the active Owen Transform Fault is an almost pure left-lateral strike-slip system with a small component of compression.
- Calibration of the sediment infill within the transform fault valley allows resolving the successive tectonic regimes with a high resolution for the recent time (post ~8.6 Ma). The Owen Transform Fault experienced a period of relative tectonic quiescence interrupted abruptly around 2.4–1.5 Ma by transpression. The switch to the new regime is marked by a ubiquitous unconformity recognized in seismic along the entire length of the fault, coeval with the uplift and folding of the sediments and the abandonment of a distributed off-ridge normal faults network. Transpression is still active today, the component of compression being accommodated by a series of secondary folds and reverse faults.

- Switch in the tectonic regime from quiescence to transpression most probably accompanied by a slight change in the India-Somalia kinematics. A 1°–4° counter-clockwise rotation in the Carlsberg spreading direction is compatible with our observations and measurements. Such small changes are difficult to detect through plate reconstructions based on magnetic anomalies since their signature remains hidden in the noise. The regional significance of this change remains elusive due to the scarcity of high-resolution data at other accreting boundaries in the Indian Ocean.
- The southernmost portion of the transform fault located near the Carlsberg-Owen RTI deviates up to ∼17° from any India-Somalia small circles, due to the recent westward propagation of the Carlsberg Ridge tip into the Somalian plate, coeval with the initiation of transpression. Such a configuration is kinematically unstable and points to a non-rigid behavior, as predicted in numerical models of long-offset transform faults. The southern Owen Ridge may be regarded as a model for the early formation of median ridges.
- Based on these new results and previous works, we propose a set of reconstructions starting shortly after the initiation of the Owen Transform Fault around Chron 6 (∼20 Ma) up to the present day. We relate the fundamental asymmetry of the Owen Transform Fault to its peculiar initiation at the tip of the Carlsberg Ridge, with distinct evolution of its southern (Carlsberg's tip) and northern (Sheba's tip) RTIs. The southern RTI has been brushing the cold Jurassic to Early Cretaceous lithosphere of the North Somali Basin until recently, resulting in particularly cold conditions around it. The abnormally deep basement close to the transform fault provides the necessary accommodation space for the Indus-derived sediments, maintaining the Transform Fault Valley as a steady-state deep flexural basin.

Data Availability Statement

The raw seismic data as well as the multibeam bathymetry used in this paper can be found online on the open data repository Janin et al. (2023).

Acknowledgments
The VARUNA (https://doi.org/10.17600/18001108) and CARLMAG (https://doi.org/10.17600/18000872) projects have been supported by the French oceanographic fleet for scientific evaluation and ship-time attribution, and by CNRS/INSU and the Geological Laboratory of Ecole normale supérieure for logistic fundings. French Navy operated the BHO Beautemps-Beaupré and handled security issues. The French Naval Hydrographic and Oceanographic Services (SHOM) coordinated pre-cruises logistics and took care of scientific instruments and data acquisition while at sea. Seismic acquisition was handled by GENAVIR (IFREMER) and seismic data were processed using CGG Geovation software. We thank Javier Escartin and Cédric Bulois for fruitful discussions and Yu Ren for his constructive review. Careful reviews by anonymous reviewers helped improve the early versions of this manuscript.

References

Agius, M., Harmon, N., Rychert, C., Tharimena, S., & Kendall, J.-M. (2018). Sediment characterization at the equatorial Mid-Atlantic Ridge from P-to-S teleseismic phase conversions recorded on the PI-LAB experiment. *Geophysical Research Letters*, *45*(22), 12–244. https://doi.org/10.1029/2018GL080565

Angelier, J., Bergerat, F., & Homberg, C. (2000). Variable coupling across weak oceanic transform fault: Flateyjarskagi, Iceland. *Terra Nova*, *12*(3), 97–101. https://doi.org/10.1046/j.1365-3121.2000.123279.x

Becker, J. J., Sandwell, D. T., Smith, W. H. F., Braud, J., Binder, B., Depner, J. L., et al. (2009). Global bathymetry and elevation data at 30 arc seconds resolution: SRTM30_PLUS. *Marine Geodesy*, *32*(4), 355–371. https://doi.org/10.1080/01490410903297766

Behn, M. D., Boettcher, M. S., & Hirth, G. (2007). Thermal structure of oceanic transform faults. *Geology*, *35*(4), 307–310. https://doi.org/10.1130/G23112A.1

Behn, M. D., & Ito, G. (2008). Magmatic and tectonic extension at mid-ocean ridges: 1. Controls on fault characteristics. *Geochemistry, Geophysics, Geosystems*, *9*(8), Q08O10. https://doi.org/10.1029/2008GC001965

Behn, M. D., Lin, J., & Zuber, M. T. (2002). Evidence for weak oceanic transform faults. *Geophysical Research Letters*, *29*(24), 60–61. https://doi.org/10.1029/2002GL015612

Bellahsen, N., Faccenna, C., Funiciello, F., Daniel, J., & Jolivet, L. (2003). Why did Arabia separate from Africa? Insights from 3-D laboratory experiments. *Earth and Planetary Science Letters*, *216*(3), 365–381. https://doi.org/10.1016/S0012-821X(03)00516-8

Bergman, E. A., Nábělek, J. L., & Solomon, S. C. (1984). An extensive region of off-ridge normal-faulting earthquakes in the southern Indian Ocean. *Journal of Geophysical Research*, *89*(B4), 2425–2443. https://doi.org/10.1029/JB089iB04p02425

Bird, P. (2003). An updated digital model of plate boundaries. *Geochemistry, Geophysics, Geosystems*, *4*(3), 1027. https://doi.org/10.1029/2001GC000252

Bonatti, E. (1976). Serpentinite protrusions in the oceanic crust. *Earth and Planetary Science Letters*, *32*(2), 107–113. https://doi.org/10.1016/0012-821X(76)90048-0

Bonatti, E. (1978). Vertical tectonism in oceanic fracture zones. *Earth and Planetary Science Letters*, *37*(3), 369–379. https://doi.org/10.1016/0012-821X(78)90052-3

Bonatti, E., Brunelli, D., Buck, W. R., Cipriani, A., Fabretti, P., Ferrante, V., et al. (2005). Flexural uplift of a lithospheric slab near the Vema transform (Central Atlantic): Timing and mechanisms. *Earth and Planetary Science Letters*, *240*(3–4), 642–655. https://doi.org/10.1016/j.epsl.2005.10.010

Bonatti, E., & Hamlyn, P. R. (1978). Mantle uplifted block in the western Indian Ocean. *Science*, *201*(4352), 249–251. https://doi.org/10.1126/science.201.4352.249

Bonatti, E., Ligi, M., Brunelli, D., Cipriani, A., Fabretti, P., Ferrante, V., et al. (2003). Mantle thermal pulses below the Mid-Atlantic Ridge and temporal variations in the formation of oceanic lithosphere. *Nature*, *423*(6939), 499–505. https://doi.org/10.1038/nature01594

Bonatti, E., Ligi, M., Gasperini, L., Peyve, A., Raznitsin, Y. U., & Chen, Y. J. (1994). Transform migration and vertical tectonics at the Romanche fracture zone, equatorial Atlantic. *Journal of Geophysical Research*, *99*(B11), 21779–21802. https://doi.org/10.1029/94JB01178

Bonatti, E., Simmons, E. C., Breger, D., Hamlyn, P., & Lawrence, J. (1983). Ultramafic rock/seawater interaction in the oceanic crust: Mg-Silicate (sepiolite) deposit from the Indian Ocean floor. *Earth and Planetary Science Letters*, *62*(2), 229–238. https://doi.org/10.1016/0012-821X(83)90086-9

Bosworth, W., Huchon, P., & McClay, K. (2005). The red sea and Gulf of Aden basins. *Journal of African Earth Sciences*, *43*(1–3), 334–378. https://doi.org/10.1016/j.jafrearsci.2005.07.020

Braun, J., & Beaumont, C. (1995). Three-dimensional numerical experiments of strain partitioning at oblique plate boundaries: Implications for contrasting tectonic styles in the southern Coast Ranges, California, and central South Island, New Zealand. *Journal of Geophysical Research*, *100*(B9), 18059–18074. https://doi.org/10.1029/95JB01683

Buck, W. R., Lavier, L. L., & Poliakov, A. N. (2005). Modes of faulting at mid-ocean ridges. *Nature*, *434*(7034), 719–723. https://doi.org/10.1038/nature03358

Bull, J., DeMets, C., Krishna, K., Sanderson, D., & Merkouriev, S. (2010). Reconciling plate kinematic and seismic estimates of lithospheric convergence in the central Indian Ocean. *Geology*, *38*(4), 307–310. https://doi.org/10.1130/G30521.1

Cande, S. C., Raymond, C. A., Stock, J., & Haxby, W. F. (1995). Geophysics of the Pitman fracture zone and Pacific-Antarctic plate motions during the Cenozoic. *Science*, *270*(5238), 947–953. https://doi.org/10.1126/science.270.5238.947

Cann, J. R., Blackman, D. K., Smith, D. K., McAllister, E., Janssen, B., Mello, S., et al. (1997). Corrugated slip surfaces formed at ridge–transform intersections on the Mid-Atlantic Ridge. *Nature*, *385*(6614), 329–332. https://doi.org/10.1038/385329a0

Carter, A., Najman, Y., Bahroudi, A., Bown, P., Garzanti, E., & Lawrence, R. D. (2010). Locating earliest records of orogenesis in western Himalaya: Evidence from Paleogene sediments in the Iranian Makran region and Pakistan Katawaz basin. *Geology*, *38*(9), 807–810. https://doi.org/10.1130/G31087.1

Chamot-Rooke, N., & Fournier, M. (2009). Tracking Arabia-India motion from Miocene to present. In *AGU fall meeting abstracts* (Vol. 2009, p. T53G–01).

Chaubey, A. K., Bhattacharya, G. C., Murty, G. P. S., Srinivas, K., Ramprasad, T., & Rao, D. G. (1998). Early Tertiary seafloor spreading magnetic anomalies and paleo-propagators in the northern Arabian Sea. *Earth and Planetary Science Letters*, *154*(1–4), 41–52. https://doi.org/10.1016/S0012-821X(97)00178-7

Chaubey, A. K., Dyment, J., Bhattacharya, G. C., Royer, J.-Y., Srinivas, K., & Yatheesh, V. (2002). Paleogene magnetic isochrons and palaeo-propagators in the Arabian and Eastern Somali basins, NW Indian Ocean. *Geological Society, London, Special Publications*, *195*(1), 71–85. https://doi.org/10.1144/GSL.SP.2002.195.01.05

Clift, P., Gaedicke, C., Edwards, R., Lee, J. I., Hildebrand, P., Amjad, S., et al. (2002). The stratigraphic evolution of the Indus Fan and the history of sedimentation in the Arabian Sea. *Marine Geophysical Researches*, *23*(3), 223–245. https://doi.org/10.1023/A:1023627123093

Clift, P. D. (2006). Controls on the erosion of Cenozoic Asia and the flux of clastic sediment to the ocean. *Earth and Planetary Science Letters*, *241*(3–4), 571–580. https://doi.org/10.1016/j.epsl.2005.11.028

Clift, P. D., Shimizu, N., Layne, G. D., Blusztajn, J. S., Gaedicke, C., Schlüter, H.-U., et al. (2001). Development of the Indus fan and its significance for the erosional history of the Western Himalaya and Karakoram. *Geological Society of America Bulletin*, *113*(8), 1039–1051. https://doi.org/10.1130/0016-7606(2001)113¡1039:DOTIFA¿2.0.CO;2

Cochran, J. R. (1981). The Gulf of Aden: Structure and evolution of a young ocean basin and continental margin. *Journal of Geophysical Research*, *86*(B1), 263–287. https://doi.org/10.1029/JB086iB01p00263

Cochran, J. R. (1988). Somali basin, Chain Ridge, and origin of the Northern Somali basin gravity and geoid low. *Journal of Geophysical Research*, *93*(B10), 11985–12008. https://doi.org/10.1029/JB093iB10p11985

Collette, B. J. (1974). Thermal contraction joints in a spreading seafloor as origin of fracture zones. *Nature*, *251*(5473), 299–300. https://doi.org/10.1038/251299a0

Cormier, M.-H., & Sloan, H. (2019). Distinctive seafloor fabric produced near western versus eastern ridge-transform intersections of the northern Mid-Atlantic Ridge: Possible influence of ridge migration. *Geochemistry, Geophysics, Geosystems*, *20*(4), 1734–1755. https://doi.org/10.1029/2018GC008101

Croon, M. B., Cande, S. C., & Stock, J. M. (2010). Abyssal hill deflections at Pacific-Antarctic ridge-transform intersections. *Geochemistry, Geophysics, Geosystems*, *11*(11), Q11004. https://doi.org/10.1029/2010GC003236

Davies, T. A., Kidd, R. B., & Ramsay, A. T. (1995). A time-slice approach to the history of Cenozoic sedimentation in the Indian Ocean. *Sedimentary Geology*, *96*(1–2), 157–179. https://doi.org/10.1016/0037-0738(94)00131-D

Delescluse, M., Montési, L., & Chamot-Rooke, N. (2008). Fault reactivation and selective abandonment in the oceanic lithosphere. *Geophysical Research Letters*, *35*(16), L16312. https://doi.org/10.1029/2008GL035066

DeMets, C., Gordon, R. G., & Argus, D. F. (2010). Geologically current plate motions. *Geophysical Journal International*, *181*(1), 1–80. https://doi.org/10.1111/j.1365-246X.2009.04491.x

DeMets, C., & Merkouriev, S. (2021). Detailed reconstructions of India–Somalia plate motion, 60 Ma to present: Implications for Somalia plate absolute motion and India–Eurasia plate motion. *Geophysical Journal International*, *227*(3), 1730–1767. https://doi.org/10.1093/gji/ggab295

DeMets, C., Merkouriev, S., & Jade, S. (2020). High-resolution reconstructions and GPS estimates of India–Eurasia and India–Somalia plate motions: 20 Ma to the present. *Geophysical Journal International*, *220*(2), 1149–1171. https://doi.org/10.1093/gji/ggz508

Dick, H. J. (1991). Tectonic evolution of the Atlantis II fracture zone. *Proceedings of Ocean Drilling Program Scientific Results Volume*, *118*, 359–398.

Dyment, J. (1998). Evolution of the Carlsberg Ridge between 60 and 45 Ma: Ridge propagation, spreading asymmetry, and the Deccan-Reunion hotspot. *Journal of Geophysical Research*, *103*(B10), 24067–24084. https://doi.org/10.1029/98JB01759

Dziewonski, A. M., Chou, T.-A., & Woodhouse, J. H. (1981). Determination of earthquake source parameters from waveform data for studies of global and regional seismicity. *Journal of Geophysical Research*, *86*(B4), 2825–2852. https://doi.org/10.1029/JB086iB04p02825

Edwards, R., Minshull, T., & White, R. (2000). Extension across the Indian–Arabian plate boundary: The Murray Ridge. *Geophysical Journal International*, *142*(2), 461–477. https://doi.org/10.1046/j.1365-246x.2000.00163.x

Ekström, G., Nettles, M., & Dziewoński, A. (2012). The global CMT project 2004–2010: Centroid-moment tensors for 13,017 earthquakes. *Physics of the Earth and Planetary Interiors*, *200*, 1–9. https://doi.org/10.1016/j.pepi.2012.04.002

Fossen, H., & Tikoff, B. (1993). The deformation matrix for simultaneous simple shearing, pure shearing and volume change, and its application to transpression-transtension tectonics. *Journal of Structural Geology*, *15*(3–5), 413–422. https://doi.org/10.1016/0191-8141(93)90137-Y

Fossen, H., & Tikoff, B. (1998). Extended models of transpression and transtension, and application to tectonic settings. *Geological Society, London, Special Publications*, *135*(1), 15–33. https://doi.org/10.1144/GSL.SP.1998.135.01.02

Fournier, M., Chamot-Rooke, N., Petit, C., Huchon, P., Al-Kathiri, A., Audin, L., et al. (2010). Arabia-Somalia plate kinematics, evolution of the Aden-Owen-Carlsberg triple junction, and opening of the Gulf of Aden. *Journal of Geophysical Research*, *115*(B4), B04102. https://doi.org/10.1029/2008JB006257

Fournier, M., Chamot-Rooke, N., Rodriguez, M., Huchon, P., Petit, C., Beslier, M.-O., & Zaragosi, S. (2011). Owen fracture zone: The Arabia–India plate boundary unveiled. *Earth and Planetary Science Letters*, *302*(1–2), 247–252. https://doi.org/10.1016/j.epsl.2010.12.027

Fournier, M., Huchon, P., Khanbari, K., & Leroy, S. (2007). Segmentation and along-strike asymmetry of the passive margin in Socotra, eastern Gulf of Aden: Are they controlled by detachment faults? *Geochemistry, Geophysics, Geosystems*, *8*(3), Q03007. https://doi.org/10.1029/2006GC001526

Fox, P. J., & Gallo, D. G. (1984). A tectonic model for ridge-transform-ridge plate boundaries: Implications for the structure of oceanic lithosphere. *Tectonophysics*, *104*(3–4), 205–242. https://doi.org/10.1016/0040-1951(84)90124-0

Gaedicke, C., Prexl, A., Schlüter, H.-U., Meyer, H., Roeser, H., & Clift, P. (2002). Seismic stratigraphy and correlation of major regional unconformities in the northern Arabian Sea. *Geological Society, London, Special Publications*, *195*(1), 25–36. https://doi.org/10.1144/GSL.SP.2002.195.01.03

Géli, L., Bougault, H., Aslanian, D., Briais, A., Dosso, L., Etoubleau, J., et al. (1997). Evolution of the Pacific-Antarctic Ridge south of the Udintsev fracture zone. *Science*, *278*(5341), 1281–1284. https://doi.org/10.1126/science.278.5341.1281

Goff, J. A., Ma, Y., Shah, A., Cochran, J. R., & Sempéré, J.-C. (1997). Stochastic analysis of seafloor morphology on the flank of the Southeast Indian Ridge: The influence of ridge morphology on the formation of abyssal hills. *Journal of Geophysical Research*, *102*(B7), 15521–15534. https://doi.org/10.1029/97JB00781

Gregory, E. P., Singh, S. C., Marjanović, M., & Wang, Z. (2021). Serpentinized peridotite versus thick mafic crust at the Romanche oceanic transform fault. *Geology*, *49*(9), 1132–1136. https://doi.org/10.1130/G49097.1

Grevemeyer, I., Rüpke, L. H., Morgan, J. P., Iyer, K., & Devey, C. W. (2021). Extensional tectonics and two-stage crustal accretion at oceanic transform faults. *Nature*, *591*(7850), 402–407. https://doi.org/10.1038/s41586-021-03278-9

Guo, Z., Liu, S., Rüpke, L., Grevemeyer, I., Morgan, J. P., Lange, D., et al. (2023). Disparate crustal thicknesses beneath oceanic transform faults and adjacent fracture zones revealed by gravity anomalies. *Geology*, *51*(3), 300–304. https://doi.org/10.1130/G50429.1

Hamlyn, P. R., & Bonatti, E. (1980). Petrology of mantle-derived ultramafics from the Owen fracture zone, northwest Indian Ocean: Implications for the nature of the oceanic upper mantle. *Earth and Planetary Science Letters*, *48*(1), 65–79. https://doi.org/10.1016/0012-821X(80)90171-5

Harmon, N., Rychert, C., Agius, M., Tharimena, S., Le Bas, T., Kendall, J. M., & Constable, S. (2018). Marine geophysical investigation of the Chain Fracture Zone in the equatorial Atlantic from the PI-LAB experiment. *Journal of Geophysical Research: Solid Earth*, *123*(12), 11–016. https://doi.org/10.1029/2018JB015982

Harmon, N., Rychert, C. A., Kendall, J. M., Agius, M., Bogiatzis, P., & Tharimena, S. (2020). Evolution of the oceanic lithosphere in the equatorial Atlantic from Rayleigh wave tomography, evidence for small-scale convection from the PI-LAB experiment. *Geochemistry, Geophysics, Geosystems*, *21*(9), e2020GC009. https://doi.org/10.1029/2020gc009174

Hubert-Ferrari, A., King, G., Manighetti, I., Armijo, R., Meyer, B., & Tapponnier, P. (2003). Long-term elasticity in the continental lithosphere; modelling the Aden Ridge propagation and the Anatolian extrusion process. *Geophysical Journal International*, *153*(1), 111–132. https://doi.org/10.1046/j.1365-246X.2003.01872.x

Iaffaldano, G., Bodin, T., & Sambridge, M. (2012). Reconstructing plate-motion changes in the presence of finite-rotations noise. *Nature Communications*, *3*(1), 1–6. https://doi.org/10.1038/ncomms2051

Iaffaldano, G., Hawkins, R., Bodin, T., & Sambridge, M. (2014). REDBACK: Open-source software for ef2waficient noise-reduction in plate kinematic reconstructions. *Geochemistry, Geophysics, Geosystems*, *15*(4), 1663–1670. https://doi.org/10.1002/2014GC005309

International Seismological Centre. (2021). *On-line bulletin*. International Seismological Centre Thatcham. https://doi.org/10.31905/D808B830

Jacob, J., Dyment, J., & Yatheesh, V. (2014). Revisiting the structure, age, and evolution of the Wharton Basin to better understand subduction under Indonesia. *Journal of Geophysical Research: Solid Earth*, *119*(1), 169–190. https://doi.org/10.1002/2013JB010285

Janin, A., Chamot-Rooke, N., Delescluse, M., Fournier, M., Olive, J.-A., Rabaute, A., et al. (2023). Raw seismic reflection data across and along the active Owen Transform Fault (Indian Ocean) [Dataset]. OSF. https://osf.io/9r2jq/?view_only=38475fbd02aa405998ef02951658521d

Jipa, D., & Kidd, R. B. (1974). Sedimentation of coarser grained interbeds in the Arabian Sea and sedimentation processes of the Indus cone. In R. B. Whitmarsh, O. E. Weser, D. A. Ross, et al. (Eds.), *Initial Reports of the Deep Sea Drilling Project* (Vol. 23(10), pp. 471–495). U.S. Government Printing Office). https://doi.org/10.2973/dsdp.proc.23.110.1974

Kohli, A., Wolfson-Schwehr, M., Prigent, C., & Warren, J. M. (2021). Oceanic transform fault seismicity and slip mode influenced by seawater infiltration. *Nature Geoscience*, *14*(8), 606–611. https://doi.org/10.1038/s41561-021-00778-1

Kohli, A. H., & Warren, J. M. (2020). Evidence for a deep hydrologic cycle on oceanic transform faults. *Journal of Geophysical Research: Solid Earth*, *125*(2), e2019JB017. https://doi.org/10.1029/2019JB017751

Kolla, V., & Coumes, F. (1987). Morphology, internal structure, seismic stratigraphy, and sedimentation of Indus Fan. *AAPG Bulletin*, *71*(6), 650–677. https://doi.org/10.1306/94887889-1704-11D7-8645000102C1865D

Kumar, R. R., & Gordon, R. G. (2009). Horizontal thermal contraction of oceanic lithosphere: The ultimate limit to the rigid plate approximation. *Journal of Geophysical Research*, *114*(B1), B01403. https://doi.org/10.1029/2007JB005473

Leroy, S., Razin, P., Autin, J., Bache, F., d'Acremont, E., Watremez, L., et al. (2012). From rifting to oceanic spreading in the Gulf of Aden: A synthesis. *Arabian Journal of Geosciences*, *5*(5), 859–901. https://doi.org/10.1007/978-3-642-30609-9_20

Ligi, M., Bonatti, E., Gasperini, L., & Poliakov, A. N. B. (2002). Oceanic broad multifault transform plate boundaries. *Geology*, *30*(1), 11–14. https://doi.org/10.1130/0091-7613(2002)030¡0011:OBMTPB¿2.0.CO;2

Lodolo, E., Coren, F., & Ben-Avraham, Z. (2013). How do long-offset oceanic transforms adapt to plate motion changes? The example of the Western Pacific-Antarctic plate boundary. *Journal of Geophysical Research: Solid Earth*, *118*(3), 1195–1202. https://doi.org/10.1093/gji/ggt463

Macario, A., Haxby, W. F., Goff, J. A., Ryan, W. B., Cande, S. C., & Raymond, C. A. (1994). Flow line variations in abyssal hill morphology for the Pacific-Antarctic Ridge at 65 S. *Journal of Geophysical Research*, *99*(B9), 17921–17934. https://doi.org/10.1029/94JB01409

MacLeod, C. J., Searle, R., Murton, B., Casey, J., Mallows, C., Unsworth, S., et al. (2009). Life cycle of oceanic core complexes. *Earth and Planetary Science Letters*, *287*(3–4), 333–344. https://doi.org/10.1016/j.epsl.2009.08.016

Maia, M. (2019). Topographic and morphologic evidences of deformation at oceanic transform faults: Far-field and local-field stresses. In *Transform plate boundaries and fracture zones* (pp. 61–87). Elsevier. https://doi.org/10.1016/B978-0-12-812064-4.00003-7

Maia, M., Sichel, S., Briais, A., Brunelli, D., Ligi, M., Ferreira, N., et al. (2016). Extreme mantle uplift and exhumation along a transpressive transform fault. *Nature Geoscience*, *9*(8), 619–623. https://doi.org/10.1038/ngeo2759

Mallik, T. K. (1974). Heavy mineral studies of samples from deep sea drill cores of sites 223 and 224, Leg 24, Glomar Challenger cruise in the Arabian Sea. In R. B. Whitmarsh, O. E. Weser, D. A. Ross, et al. (Eds.), *Initial reports of deep sea drilling project* (Vol. 23(11), pp. 497–502). U.S. Government Printing Office. https://doi.org/10.2973/dsdp.proc.23.111.1974

Manighetti, I., Tapponnier, P., Courtillot, V., Gruszow, S., & Gillot, P.-Y. (1997). Propagation of rifting along the Arabia-Somalia plate boundary: The Gulfs of Aden and Tadjoura. *Journal of Geophysical Research*, *102*(B2), 2681–2710. https://doi.org/10.1029/96JB01185

Marjanović, M., Singh, S. C., Gregory, E. P., Grevemeyer, I., Growe, K., Wang, Z., et al. (2020). Seismic crustal structure and morphotectonic features associated with the Chain Fracture Zone and their role in the evolution of the equatorial Atlantic region. *Journal of Geophysical Research: Solid Earth*, *125*(10), e2020JB020. https://doi.org/10.1029/2020JB020275

McCarthy, M. C., Kruse, S. E., Brudzinski, M. R., & Ranieri, M. E. (1996). Changes in plate motions and the shape of Pacific fracture zones. *Journal of Geophysical Research*, *101*(B6), 13715–13730. https://doi.org/10.1029/96JB00646

McQuarrie, N., Stock, J., Verdel, C., & Wernicke, B. (2003). Cenozoic evolution of Neotethys and implications for the causes of plate motions. *Geophysical Research Letters*, *30*(20), 2036. https://doi.org/10.1029/2003GL017992
Menard, H. W., & Atwater, T. (1969). Origin of fracture zone topography. *Nature*, *222*(5198), 1037–1040. https://doi.org/10.1038/2221037a0
Mercuriev, S., Patriat, P., & Sochevanova, N. (1995). Évolution de la dorsale de Carlsberg: évidence pour une phase d'expansion très lente entre 40 et 25 Ma (A18 à A7). *Oceanologica Acta*, *19*(1), 1–13.
Merkouriev, S., & DeMets, C. (2006). Constraints on Indian plate motion since 20 Ma from dense Russian magnetic data: Implications for Indian plate dynamics. *Geochemistry, Geophysics, Geosystems*, *7*(2), Q02002. https://doi.org/10.1029/2005GC001079
Mishra, J. K., & Gordon, R. G. (2016). The rigid-plate and shrinking-plate hypotheses: Implications for the azimuths of transform faults. *Tectonics*, *35*(8), 1827–1842. https://doi.org/10.1002/2015TC003968
Mishra, R., Pandey, D. K., Ramesh, P., & Clift, P. D. (2016). Identification of new deep sea sinuous channels in the eastern Arabian Sea. *SpringerPlus*, *5*(1), 1–18. https://doi.org/10.1186/s40064-016-2497-6
Morgan, J. P., & Parmentier, E. M. (1984). Lithospheric stress near a ridge-transform intersection. *Geophysical Research Letters*, *11*(2), 113–116. https://doi.org/10.1029/GL011i002p00113
Mountain, G., & Prell, W. (1990). A multiphase plate tectonic history of the southeast continental margin of Oman. *Geological Society, London, Special Publications*, *49*(1), 725–743. https://doi.org/10.1144/GSL.SP.1992.049.01.44
Najman, Y. (2006). The detrital record of orogenesis: A review of approaches and techniques used in the Himalayan sedimentary basins. *Earth-Science Reviews*, *74*(1–2), 1–72. https://doi.org/10.1016/j.earscirev.2005.04.004
Neuharth, D., Brune, S., Glerum, A., Morley, C. K., Yuan, X., & Braun, J. (2021). Flexural strike-slip basins. *Geology*, *50*(3), 361–365. https://doi.org/10.1130/G49351.1
Olive, J.-A., Behn, M. D., & Tucholke, B. E. (2010). The structure of oceanic core complexes controlled by the depth distribution of magma emplacement. *Nature Geoscience*, *3*(7), 491–495. https://doi.org/10.1038/ngeo888
Parmentier, E., & Haxby, W. (1986). Thermal stresses in the oceanic lithosphere: Evidence from geoid anomalies at fracture zones. *Journal of Geophysical Research*, *91*(B7), 7193–7204. https://doi.org/10.1029/JB091iB07p07193
Patriat, P., & Achache, J. (1984). India–Eurasia collision chronology has implications for crustal shortening and driving mechanism of plates. *Nature*, *311*(5987), 615–621. https://doi.org/10.1038/311615a0
Perch-Nielsen, K., Supko, P. R., Boersma, A., Bonatti, E., Carlson, R. L., McCoy, F., et al. (1977). Site 353; Vema Fracture Zone. In *Initial reports of the deep sea drilling project* (Vol. 39, pp. 27–44). Texas A and M University, Ocean Drilling Program. https://doi.org/10.2973/dsdp.proc.39.102.1977
Pinzón, N., & Vargas, C. A. (2021). Global variation of seismic energy release with oceanic lithosphere age. *Scientific Reports*, *11*(1), 1–9. https://doi.org/10.1038/s41598-020-80475-y
Pockalny, R. A. (1997). Evidence of transpression along the Clipperton Transform: Implications for processes of plate boundary reorganization. *Earth and Planetary Science Letters*, *146*(3–4), 449–464. https://doi.org/10.1016/S0012-821X(96)00253-1
Pockalny, R. A., Detrick, R. S., & Fox, P. J. (1988). Morphology and tectonics of the Kane transform from Sea Beam bathymetry data. *Journal of Geophysical Research*, *93*(B4), 3179–3193. https://doi.org/10.1029/JB093iB04p03179
Pockalny, R. A., Fox, P. J., Fornari, D. J., Macdonald, K. C., & Perfit, M. R. (1997). Tectonic reconstruction of the Clipperton and Siqueiros Fracture Zones: Evidence and consequences of plate motion change for the last 3 Myr. *Journal of Geophysical Research*, *102*(B2), 3167–3181. https://doi.org/10.1029/96JB03391
Pockalny, R. A., Gente, P., & Buck, R. (1996). Oceanic transverse ridges: A flexural response to fracture-zone–normal extension. *Geology*, *24*(1), 71–74. https://doi.org/10.1130/0091-7613(1996)024¡0071:OTRAFR¿2.3.CO;2
Prigent, C., Warren, J. M., Kohli, A. H., & Teyssier, C. (2020). Fracture-mediated deep seawater flow and mantle hydration on oceanic transform faults. *Earth and Planetary Science Letters*, *532*, 115988. https://doi.org/10.1016/j.epsl.2019.115988
Qayyum, M., Lawrence, R. D., & Niem, A. R. (1997). Discovery of the palaeo-Indus delta-fan complex. *Journal of the Geological Society*, *154*(5), 753–756. https://doi.org/10.1144/gsjgs.154.5.0753
Qayyum, M., Niem, A. R., & Lawrence, R. D. (1996). Newly discovered Paleogene deltaic sequence in Katawaz basin, Pakistan, and its tectonic implications. *Geology*, *24*(9), 835–838. https://doi.org/10.1130/0091-7613(1996(024¡0835:NDPDSI¿2.3.CO;2
Qayyum, M., Niem, A. R., & Lawrence, R. D. (2001). Detrital modes and provenance of the Paleogene Khojak formation in Pakistan: Implications for early Himalayan orogeny and unroofing. *Geological Society of America Bulletin*, *113*(3), 320–332. https://doi.org/10.1130/0016-7606(2001)113¡0320:DMAPOT¿2.0.CO;2
Rea, D. K. (1992). Delivery of Himalayan Sediment to the Northern Indian Ocean and its relation to global climate, sea level, uplift, and seawater strontium. In R. A. Duncan, D. K. Rea, R. B. Kidd, U. von Rad, & J. K. Weissel (Eds.), *Synthesis of results from scientific drilling in the Indian ocean* (pp. 387–402). American Geophysical Union (AGU). https://doi.org/10.1029/GM070p0387
Ren, Y., Geersen, J., & Grevemeyer, I. (2022). Impact of spreading rate and age-offset on oceanic transform fault morphology. *Geophysical Research Letters*, *49*(2),e2021GL096170. https://doi.org/10.1029/2021GL096170
Rodriguez, M., Chamot-Rooke, N., Huchon, P., Fournier, M., & Delescluse, M. (2014). The Owen Ridge uplift in the Arabian Sea: Implications for the sedimentary record of Indian monsoon in Late Miocene. *Earth and Planetary Science Letters*, *394*, 1–12. https://doi.org/10.1016/j.epsl.2014.03.011
Rodriguez, M., Chamot-Rooke, N., Huchon, P., Fournier, M., Lallemant, S., Delescluse, M., et al. (2014). Tectonics of the Dalrymple trough and uplift of the Murray ridge (NW Indian Ocean). *Tectonophysics*, *636*, 1–17. https://doi.org/10.1016/j.tecto.2014.08.001
Rodriguez, M., Fournier, M., Chamot-Rooke, N., Huchon, P., Bourget, J., Sorbier, M., et al. (2011). Neotectonics of the Owen Fracture Zone (NW Indian Ocean): Structural evolution of an oceanic strike-slip plate boundary. *Geochemistry, Geophysics, Geosystems*, *12*(12), Q12006. https://doi.org/10.1029/2011GC003731
Rodriguez, M., Fournier, M., Chamot-Rooke, N., Huchon, P., & Delescluse, M. (2018). The geological evolution of the Aden-Owen-Carlsberg Triple Junction (NW Indian Ocean) since the late Miocene. *Tectonics*, *37*(5), 1552–1575. https://doi.org/10.1029/2017TC004687
Rodriguez, M., Huchon, P., Chamot-Rooke, N., Fournier, M., Delescluse, M., & François, T. (2016). Tracking the Paleogene India-Arabia plate boundary. *Marine and Petroleum Geology*, *72*, 336–358. https://doi.org/10.1016/j.marpetgeo.2016.02.019
Royer, J.-Y., Chaubey, A., Dyment, J., Bhattacharya, G., Srinivas, K., Yatheesh, V., & Ramprasad, T. (2002). Paleogene plate tectonic evolution of the Arabian and Eastern Somali basins. *Geological Society, London, Special Publications*, *195*(1), 7–23. https://doi.org/10.1144/GSL.SP.2002.195.01.02
Ryan, W. B., Carbotte, S. M., Coplan, J. O., O'Hara, S., Melkonian, A., Arko, R., et al. (2009). Global multi-resolution topography synthesis. *Geochemistry, Geophysics, Geosystems*, *10*(3), Q03014. https://doi.org/10.1029/2008GC002332
Sandwell, D., & Schubert, G. (1982). Lithospheric flexure at fracture zones. *Journal of Geophysical Research*, *87*(B6), 4657–4667. https://doi.org/10.1029/JB087iB06p04657

Sandwell, D. T. (1986). Thermal stress and the spacings of transform faults. *Journal of Geophysical Research*, *91*(B6), 6405–6417. https://doi.org/10.1029/JB091iB06p06405

Severinghaus, J. P., & Macdonald, K. C. (1988). High inside corners at ridge-transform intersections. *Marine Geophysical Researches*, *9*(4), 353–367. https://doi.org/10.1007/BF00315005

Shipboard Scientific Party. (1989a). Site 720. In W. L. Prell & N. Niitsuma (Eds.), *Proc. ODP, Init. Repts*, (Vol. 117, pp. 157–195). Ocean Drilling Program). https://doi.org/10.2973/odp.proc.ir.117.104.1989

Shipboard Scientific Party. (1989b). Site 721. In W. L. Prell & N. Niitsuma (Eds.), *Proc. ODP, Init. Repts* (Vol. 117, pp. 197–254). Ocean Drilling Program). https://doi.org/10.2973/odp.proc.ir.117.106.1989

Shipboard Scientific Party. (1989c). Site 722. In W. L. Prell & N. Niitsuma (Eds.), *Proc. ODP, Init. Repts* (Vol. 117, pp. 255–317). Ocean Drilling Program). https://doi.org/10.2973/odp.proc.ir.117.107.1989

Shipboard Scientific Party. (1989d). Site 731. In W. L. Prell & N. Niitsuma (Eds.), *Proc. ODP, Init. Repts* (Vol. 117, pp. 585–652). Ocean Drilling Program). https://doi.org/10.2973/odp.proc.ir.117.108.1989

Sonder, L. J., & Pockalny, R. A. (1999). Anomalously rotated abyssal hills along active transforms: Distributed deformation of oceanic lithosphere. *Geology*, *27*(11), 1003–1006. https://doi.org/10.1130/0091-7613(1999)027¡1003:ARAHAA¿2.3.CO;2

Steckler, M. S., & ten Brink, U. S. (1986). Lithospheric strength variations as a control on new plate boundaries: Examples from the northern Red Sea region. *Earth and Planetary Science Letters*, *79*(1–2), 120–132. https://doi.org/10.1016/0012-821X(86)90045-2

Stein, C. A., & Cochran, J. R. (1985). The transition between the Sheba Ridge and Owen Basin: Rifting of old oceanic lithosphere. *Geophysical Journal International*, *81*(1), 47–74. https://doi.org/10.1111/j.1365-246X.1985.tb01350.x

Stein, C. A., & Stein, S. (1992). A model for the global variation in oceanic depth and heat flow with lithospheric age. *Nature*, *359*(6391), 123–129. https://doi.org/10.1038/359123a0

Stevens, D. E., McNeill, L. C., Henstock, T. J., Delescluse, M., Chamot-Rooke, N., & Bull, J. M. (2020). A complete structural model and kinematic history for distributed deformation in the Wharton Basin. *Earth and Planetary Science Letters*, *538*, 116218. https://doi.org/10.1016/j.epsl.2020.116218

Stoddard, P. R., & Stein, S. (1988). A kinematic model of ridge-transform geometry evolution. *Marine Geophysical Researches*, *10*(3–4), 181–190. https://doi.org/10.1007/BF00310063

Storchak, D. A., Harris, J., Brown, L., Lieser, K., Shumba, B., & Di Giacomo, D. (2020). Rebuild of the Bulletin of the International Seismological Centre (ISC)—Part 2: 1980–2010. *Geoscience Letters*, *7*(1), 1–21. https://doi.org/10.1186/s40562-020-00164-6

Storchak, D. A., Harris, J., Brown, L., Lieser, K., Shumba, B., Verney, R., et al. (2017). Rebuild of the Bulletin of the International Seismological Centre (ISC). Part 1: 1964–1979. *Geoscience Letters*, *4*(1), 1–14. https://doi.org/10.1186/s40562-017-0098-z

Thompson, G., & Melson, W. G. (1972). The petrology of oceanic crust across fracture zones in the Atlantic Ocean: Evidence of a new kind of sea-floor spreading. *The Journal of Geology*, *80*(5), 526–538. https://doi.org/10.1086/627779

Tréhu, A. M., Scheidhauer, M., Rohr, K. M., Tikoff, B., Walton, M. A., Gulick, S. P., & Roland, E. C. (2015). An abrupt transition in the mechanical response of the upper crust to transpression along the Queen Charlotte Fault. *Bulletin of the Seismological Society of America*, *105*(2B), 1114–1128. https://doi.org/10.1785/0120140159

Tsang-Hin-Sun, E., Royer, J.-Y., & Perrot, J. (2016). Seismicity and active accretion processes at the ultraslow-spreading Southwest and intermediate-spreading Southeast Indian ridges from hydroacoustic data. *Geophysical Journal International*, *206*(2), 1232–1245. https://doi.org/10.1093/gji/ggw201

Tucholke, B. E., & Schouten, H. (1988). Kane fracture zone. *Marine Geophysical Researches*, *10*(1), 1–39. https://doi.org/10.1007/BF02424659

Turcotte, D. L. (1974). Are transform faults thermal contraction cracks? *Journal of Geophysical Research*, *79*(17), 2573–2577. https://doi.org/10.1029/JB079i017p02573

Von Rad, U., & Tahir, M. (1997). Late Quaternary sedimentation on the outer Indus shelf and slope (Pakistan): Evidence from high-resolution seismic data and coring. *Marine Geology*, *138*(3–4), 193–236. https://doi.org/10.1016/S0025-3227(96)00090-4

Weedon, G., & McCave, I. (1991). Mud turbidites from the Oligocene and Miocene Indus fan at sites 722 and 731 on the Owen Ridge. In W. L. Prell, N. Niitsuma, et al. (Eds.), *Proceedings of the ocean drilling program, scientific results* (Vol. 117(10), pp. 215–220). Ocean Drilling Program). https://doi.org/10.2973/odp.proc.sr.117.140.1991

Weser, O. E. (1974). Sedimentological aspects of strata encountered on Leg 23 in the northern Arabian Sea. In R. B. Whitmarsh, O. E. Weser, D. A. Ross, et al. (Eds.), *Initial reports of deep sea drilling project* (Vol. 23(12), pp. 503–519). U.S. Government Printing Office. https://doi.org/10.2973/dsdp.proc.23.112.1974

Wessel, P., & Haxby, W. F. (1990). Thermal stresses, differential subsidence, and flexure at oceanic fracture zones. *Journal of Geophysical Research*, *95*(B1), 375–391. https://doi.org/10.1029/JB095iB01p00375

Whitmarsh, R. B., Weser, O. E., Ali, S., Boudreaux, J. E., Fleisher, R. L., Jipa, D., et al. (1974a). Site 224. In R. B. Whitmarsh, O. E. Weser, & D. A. Ross (Eds.), *Initial reports of the deep sea drilling project* (Vol. 23, pp. 383–419). U.S. Government Printing Office). https://doi.org/10.2973/dsdp.proc.23.108.1974

Whitmarsh, R. B., Weser, O. E., Ali, S., Boudreaux, J. E., Fleisher, R. L., Jipa, D., et al. (1974b). Site 221. In R. B. Whitmarsh, O. E. Weser, & D. A. Ross (Eds.), *Initial reports of the deep sea drilling project* (Vol. 23, pp. 167–210). U.S. Government Printing Office). https://doi.org/10.2973/dsdp.proc.23.105.1974

Whitmarsh, R. B., Weser, O. E., Ali, S., Boudreaux, J. E., Fleisher, R. L., Jipa, D., et al. (1974c). Site 222. In R. B. Whitmarsh, O. E. Weser, & D. A. Ross (Eds.), *Initial reports of the deep sea drilling project* (Vol. 23, pp. 211–289). U.S. Government Printing Office). https://doi.org/10.2973/dsdp.proc.23.106.1974

Wolfe, C. J., Bergman, E. A., & Solomon, S. C. (1993). Oceanic transform earthquakes with unusual mechanisms or locations: Relation to fault geometry and state of stress in the adjacent lithosphere. *Journal of Geophysical Research*, *98*(B9), 16187–16211. https://doi.org/10.1038/s41561-021-00778-1